MASTERARBEIT / MASTER'S THESIS

Titel der Masterarbeit / Title of the Master's Thesis

„HP/HT deformation experiments of garnet-omphacite aggregates – influence of volume fractions on deformation mechanisms. "

verfasst von / submitted by

Stefanie Klackl, BSc

angestrebter akademischer Grad / in partial fulfilment of the requirements for the degree of

Master of Science (MSc)

Wien, 2022 / Vienna 2022

Studienkennzahl lt. Studienblatt / degree programme code as it appears on the student record sheet:	A 066 815
Studienrichtung lt. Studienblatt / degree programme as it appears on the student record sheet:	Masterstudium Erdwissenschaften
Betreut von / Supervisor:	Dr. Anna Rogowitz

Contents

Acknowledgements

I would like to thank my supervisor Anna Rogowitz for her incredible patience and support, always making time to answer any questions, reading my numerous revisions and spending hours EBSD mapping in a cold basement with me.

I would also like to extend my sincere thanks to Katrin Kraus for performing the deformation experiments and to Ilka Wünsche for the preparations of the thin sections.

Thank you so much to my fellow students Stefanie Koppensteiner, Manuel Werdenich and Michael Nagl for productive discussions and many nice chats during lunch breaks and various other breaks.

I am so thankful to my family, who has always helped and supported me. Thanks should also go to Tanja, who has managed to survive living with me ever since first moving to Vienna. None of this would have been anywhere near as fun without her!

This study was financed by the Austrian Science Foundation (FWF) Grant number: P 29539-N29 (to AR).

Abstract

Forming in oceanic and continental subduction zones during high to ultra-high-pressure metamorphism, eclogites play an important role in convergent settings. Natural eclogites are however often overprinted by retrograde metamorphism or later deformation, making it hard to distinguish what happened at eclogite facies conditions. High-pressure high temperature deformation experiments in a Griggs-type deformation apparatus were conducted on synthetic eclogite to investigate the mechanical behaviour and link it directly to deformation mechanisms at controlled P-T conditions. To improve our understanding of eclogite deformation behaviour with respect to its phase abundance of omphacite and garnet, synthetic eclogite samples containing 25, 50 and 75% volume fraction of garnet were used in the deformation experiments. Deformation conditions were set to a confining pressure of 2.5 GPa, 900 °C and a strain rate of $3*10^{-6}$ s^{-1}. Detailed microstructure analysis via optical and electron microscope imaging (secondary electron, backscattered electron, forward scattered electron and electron backscattered diffraction) served for identification of the dominant active deformation mechanism.

The mechanical data reveals an increase of eclogite strength, with increasing garnet content. As for deformational behaviour, a change from predominantly crystal plastic deformation of omphacite to more and more brittle deformation of both phases can be observed. The main crystal plastic deformation mechanism of omphacite is dislocation creep, which is indicated by undulatory extinction, slip lines and a weak CPO. In accordance to uniaxial shortening the CPO resembles an S-type texture with a point maximum of [001] axis parallel to the foliation and a maximum of [010] axis perpendicular to the foliation. Other commonly observed crystal plastic deformation mechanisms are mechanical twinning, which decreases with increasing garnet content, and low angle grain boundaries which increase with increasing garnet content. Low angle grain boundaries, as well as smaller grain sizes and higher misorientations are commonly found around phase boundaries, indicating a localization of strain in these areas.

While garnet exhibits signs of minor plastic deformation, which increase with increasing garnet content, the main change in deformation behaviour can be observed in the change of brittle deformation behaviour. In the sample containing 25% volume fraction of garnet breaks mainly parallel to the main compressive stress. With increasing garnet content, fractures

become both more frequent, as well as more random in orientation, potentially indicating local perturbations of the stress field.

Zusammenfassung

Eklogite bilden sich in ozeanischen und kontinentalen Subduktionszonen, während der Hoch- bis Ultra-Hochdruckmetamorphose und spielen eine wichtige Rolle bei konvergierenden Plattengrenzen. Natürliche Eklogite sind jedoch oft von retrograder Metamorphose oder späterer Deformation überprägt, so dass es schwierig ist, zu bestimmen, was unter eklogitfaziellen Bedingungen geschah. Es wurden Hochdruck-Hochtemperatur-Deformationsexperimente in einem Griggs-Typ-Deformationsapparat an synthetischem Eklogit durchgeführt, um das mechanische Verhalten zu untersuchen und es direkt mit den Deformationsmechanismen unter kontrollierten P-T-Bedingungen in Verbindung zu bringen. Um unser Verständnis des Deformationsverhaltens von Eklogit im Zusammenhang mit seinen Anteilen an Omphazit und Granat zu verbessern, wurden in den Deformationsexperimenten synthetische Eklogite mit einem Volumenanteil von jeweils 25, 50 und 75 % Granat verwendet. Die Deformationsbedingungen waren ein Begrenzungsdruck von 2,5 GPa, Temperaturen von 900 °C und eine Strainrate von $3*10^{-6}s^{-1}$. Eine detaillierte Mikrostrukturanalyse mittels optischer und elektronenmikroskopischer Bildgebung (Sekundärelektronen-, Rückstreuelektronen-, Vorwärtsstreuelektronen- und Rückstreuelektronenbeugung) diente zur Identifizierung der Deformationsmechanismen.

Die mechanischen Daten zeigen eine Zunahme der Festigkeit von Eklogit mit zunehmendem Granatgehalt. Was das Deformationsverhalten anbelangt, so ist ein Wechsel von überwiegend kristallplastischer Deformation von Omphazit zu zunehmend spröder Deformation beider Phasen zu beobachten. Der Hauptmechanismus der kristallplastischen Deformation von Omphazit ist das Versetzungskriechen, worauf undulöse Auslöschung, Slip-Lines und eine schwache CPO schließen lassen. In Übereinstimmung mit der einachsigen Verkürzung ähnelt die CPO einer S-Textur mit einem Punktmaximum der [001]-Achse parallel zur Foliation und einem Maximum der [010]-Achse senkrecht zur Foliation. Andere häufig beobachtete, kristallplastische Deformationsmechanismen sind die mechanische Verzwillingung, die mit zunehmendem Granatgehalt abnimmt und Kleinwinkelkorngrenzen, die mit zunehmendem Granatgehalt zunehmen. Kleinwinkelkorngrenzen sowie kleinere Korngrößen und höhere Missorientierungen sind häufig bei Phasengrenzen zu finden, was auf eine Lokalisierung des Strains in diesen Bereichen hinweist.

Während Granat Anzeichen einer geringfügigen kristallplastischen Deformation aufweist, die mit zunehmendem Granatgehalt zunimmt, ist die auffälligere Veränderung des Deformationsverhaltens in der spröden Deformation zu beobachten. In der Probe mit einem Granatanteil von 25 % bricht der Granat hauptsächlich parallel zur Hauptdruckspannung. Mit zunehmendem Granatgehalt werden die Brüche sowohl häufiger als auch zufälliger in ihrer Ausrichtung, was möglicherweise auf lokale Störungen des Spannungsfeldes hinweist.

1. Introduction

1.1 Motivation

Eclogite, first introduced by Häuy (1822), is a mafic rock consisting predominantly of garnet and omphacite. It can also contain quartz, mica, amphibole, epidote, rutile and kyanite. Eclogite is formed by high to ultra-high-pressure metamorphism of basalt or gabbro in continental and oceanic subduction zones and is stable over a wide range of pressure and temperature conditions from about 1.2 GPa and 500 °C and above (Ringwood and Green, 1966). With ongoing subduction, the amount of garnet increases on the expense of omphacite (Zhang and Green, 2007; Green and Ringwood, 1967).

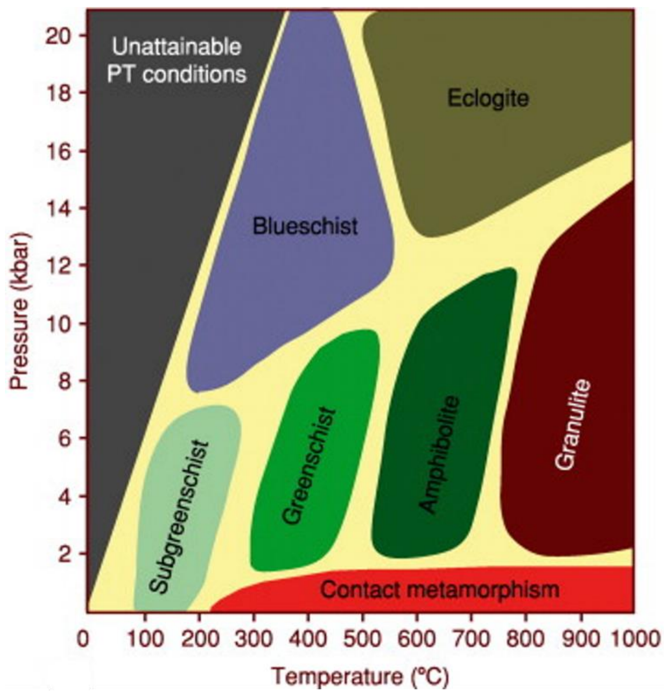

Figure 1. PT diagram of metamorphic facies by Bucher (2005)

Eclogitization is usually initiated by fluids infiltrating deep crustal layers, triggering and enhancing metamorphic reactions. The replacement of mafic protolith by the eclogitic mineral assemblage leads to an increase in density and a loss in volume potentially causing fracturing and introducing more fluid pathways, consequently enhancing eclogitization (Austrheim, 1987). Eclogitization induced density increase has been shown to be up to 14% (Rogowitz and Huet, 2021). Due to negative buoyancy forces completely eclogitized rocks should descend further into the mantle, making their exhumation impossible. Partly eclogitized rocks, however, could still be light enough to be exhumed (Jolivet et al., 2005).

One example for incomplete eclogitization is a large eclogite body in the Bergen arcs where strain localization in eclogite allowed a decoupling from the descending slab, followed by an exhumation due to buoyancy (Jolivet et al., 2005). Incomplete eclogitized bodies are also found in the Western Gneiss Region (Austrheim et al., 2003), at the Koralpe and Saualpe (Miller et al., 2007) and the Gran Paradiso nappe (Le Goff and Ballèvre, 1990) amongst others. The investigation of such exhumed eclogitic bodies can give an insight into processes active at collision and subduction zones.

However, as natural eclogites are often overprinted by retrograde metamorphism or later deformation, it can be hard to identify what happened at eclogite facies conditions. High-pressure high temperature deformation experiments in a Griggs-type deformation apparatus can help as they allow to investigate the mechanical behaviour and link it directly to deformation mechanisms at controlled P-T conditions.

1.2 Deformation mechanisms

1.2.1 Omphacite

Omphacite is a clinopyroxene between the endmembers jadeite and diopside and represents one of the major minerals in eclogite (Zhang et al., 2006). In natural eclogite omphacite has been shown to deform by crystal plastic deformation at temperatures as low as of 550 – 600 °C (Buatier et al., 1991). At higher temperatures subgrain rotation and grain boundary migration have been identified as main recrystallization mechanisms (Keppler et al., 2016). Common microstructural observations of omphacite in deformed natural eclogite are a strong shape preferred orientation (SPO) and crystallographic preferred orientation (CPO), typically interpreted as a result of crystal plasticity.

Helmstaedt et al. (1972) classified the CPOs of omphacite in natural eclogite into two main types: S- and L-type. The S-type CPO is characterized by a point maximum of [010] normal to the foliation, while [001] forms a girdle parallel to the foliation plane. The L-type CPO shows a point maximum of [001] parallel to the lineation, with [010] forming a girdle perpendicular to the lineation. Later, Godard and van Roermund (1995) added the intermediate SL- and LS-type CPOs (Fig. 1). Whereas the SL-Type is similar to the S-Type with [001] forming a girdle parallel the foliation and a point maximum of [010] normal to the foliation and the LS-type is characterized by a point maximum of [001] parallel to the lineation and a point maximum of [010] normal to the foliation. Previous studies have associated the dominant textures with strain states whereas the L-type CPO is often linked to constriction, while the S-type is associated with flattening and intermediate CPO types are closer to plain strain (Fig. 2; Keppler, 2018; Kurz, 2005).

While the observed CPOs suggest a (010) [001] slip system, transmission-electron microscope analysis has shown the dominant slip systems in omphacite to be (100) [001], {110} [001], {110} ½, and {-110} ½ (Godard and van Roermund, 1995). These contradicting observations indicate that omphacite favours multiple slip systems rather than easy slip on one slip system. Another possible origin of the observed CPOs could be diffusion creep with concomitant anisotropic growth and dissolution (Mauler et al., 2001; Stünitz et al., 2020). The latter has been identified to be favoured at lower temperatures (Godard and van Roermund, 1995).

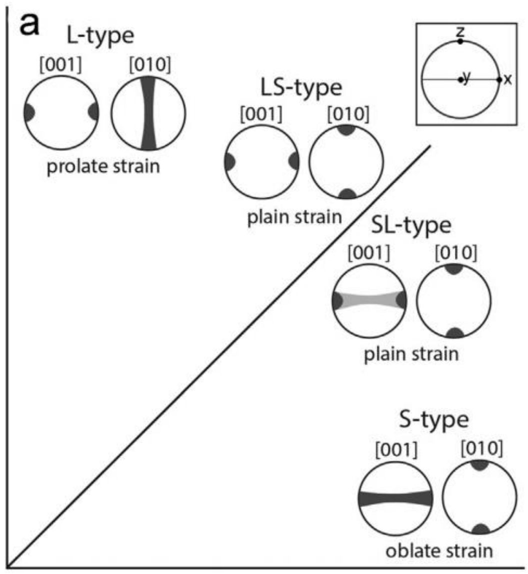

Figure 2. Flinn diagram by Keppler (2018) plotting L-type to S-type omphacite fabrics together with their interpretation in terms of strain geometry; stereo plot in upper right corner shows orientation of lineation (X) and foliation normal (Z).

Deformation experiments on omphacite aggregates have produced similar microfabrics compared to those observed in naturally deformed omphacite, again identifying {110} ½ ⟨110⟩, {110} [001] and (100) [001] as dominant slip systems (Zhang et al., 2006). It further has been shown that the creep strength of omphacite lies between that of diopside and jadeite, decreasing towards the jadeite endmember (Moghadam et al., 2010). In deformation experiments performed on natural coarse-grained clinopyroxenite and synthetic fine-grained clinopyroxenite diffusional creep was active at a lower differential stress, while dislocation creep was the dominant deformation mechanism at higher differential stress. Those experiments also showed that within the dislocation creep field the fine-grained samples generally yield creep rates about one order of magnitude faster than the coarser samples (Bystricky and Mackwell, 2001).

1.2.2 Garnet

Garnet represents the other main component of eclogite. It is the third most abundant phase in the upper mantle and is second only to ringwoodite in the transition zone from upper to lower mantle (Ringwood, 1991). The resistance of garnet to plastic deformation is higher than that of other minerals in the Earth's mantle (Karato et al., 1995). Deformation experiments on single garnet crystals have previously shown garnet to become ductile at temperatures of above 850 °C (Wang and Ji, 1999). However, naturally deformed garnet has been found to show indication of dislocation creep and thermally induced recovery at temperatures as low as 600 °C (Voegelé et al., 1998a) and at higher temperatures in deformed mantle garnet (Prior et al., 2000). Moreover, Bestmann et al. (2008) found recrystallization and diffusion accommodated grain boundary sliding to be the dominant deformation mechanism in garnet that was estimated to have deformed at temperatures of 600 to 750 °C. Aside of intracrystalline plasticity pressure solution has been found to be an important deformation mechanism of garnet (Smit et al., 2011).

In comparison, high pressure deformation experiments (Voegelé et al., 1998b) have shown brittle deformation of garnet at temperatures below 1000 °C and ductile deformation by dislocation creep with significant recovery at temperatures > 1000 °C. In a more recent experimental study, the dependency of garnet creep strength on water content has been investigated (Xu et al., 2013). Those experiments have shown that an increased water content in garnet can result in up to the three orders of magnitude faster creep rates. Typical slip systems in both, naturally and experimentally deformed garnet have been identified via transmission electron microscopy to be ½ ⟨111⟩ {11̄0}, ½ ⟨111⟩ {112}, ½ ⟨111⟩ {123}, ⟨100⟩ {010} (Voegelé, 1998a, 1998b).

1.2.3 Eclogite

The deformation behaviour of eclogite has been subject of a large number of experimental, numerical and studies on natural rocks (e.g., Austrheim, 1987; Philippot and van Roermund, 1992; Engvik et al., 2007; Angiboust et al., 2011; Yamato et al., 2019). A variety of deformation mechanism including fracturing, dislocation creep, diffusion and dissolution-reprecipitation creep and grain boundary sliding have been identified to accommodate strain in deforming eclogites (e.g., Mauler et al., 2001; Engvik et al., 2007; Zhang and Green, 2007). Which mechanism is the dominant strain accommodating mechanism depends on various factors including temperature and pressure conditions, water content, grain size and modal composition (Godard and van Roermund, 1995; Zhang and Green, 2007; Yamato et al., 2019).

Eclogites deformed at lower temperatures often reveal breccias (e.g., Angiboust et al., 2012). Especially garnet exhibits brittle deformation, while omphacite may show some crystal plastic deformation (Angiboust et al., 2011). At higher temperatures (> 600 °C) mylonitic eclogite has been identified (Engvik et al., 2007; Austrheim, 2013).

In such highly foliated, mylonitic eclogite omphacite often reveals a CPO, which has been shown to develop by dislocation creep (Engvik et al., 2007). However, in the presence of fluids diffusion and dissolution-reprecipitation creep can also produce a typical S-Type CPO in omphacite (Mauler et al., 2001; Stünitz et al., 2020; Rogowitz and Huet, 2021).

The activity of such non-dislocation-based mechanisms, including dissolution-precipitation creep and grain boundary sliding seem to be higher early during eclogitization and in fine-grained eclogite (Cao et al., 2020).

Besides grainsize, deformation conditions and fluid content, the volume fraction of components have been proven to influence eclogite deformation behaviour (Zhang and Green, 2007; Yamato et al., 2019). Numerical models suggest that at conditions where the omphacite matrix deforms in a crystal plastic manner, an increase in garnet content results in an increase of the effective stress (Yamato et al., 2019). Those observations are in accordance with previous deformation experiments which revealed an increase in strength of eclogite with increasing garnet content (Zhang and Green, 2007).

1.2.4 Two-Phase Rocks

Most rocks in the lower crust and upper mantle are polyphase, which has inspired various laboratory experiment on two-phase aggregates (eg. Jordan, 1987; Tullis et al., 1991; Ji et al., 2001). Deformation experiments have demonstrated that within uniform stress and strain rate bounds, the strength of two-phase aggregates is mainly dependent on the volume fraction of their components (Tullis et al., 1991). For example, deformation experiments conducted on calcite-quartz aggregates (Rybacki et al., 2003) have shown an increase in strength with increasing quartz content. A similar observation has been made for anorthite-diopside rocks (Dimanov and Dresen, 2005), whereas the aggregate strength is increasing with increasing diopside content. Aside of the composition, the phase distribution and potential interconnectivity of the phases can influence the strength of two-phase rocks (Handy, 1994). According to Handy (1994) deformed rocks can be described by two end-member fabrics: load bearing framework (LBF) or interconnected weak layers (IWL). The LBF comprises a strong phase containing pockets of a weak phase. Stress concentrates in the LBF and strain rates are nearly uniform. The IWL is made up of interconnected layers of a weak phase that separate boudins and clasts of a strong phase. Strain rates are higher in the interconnected weak phase than in the clasts of strong phase. The phenomenological study by Handy (1994) can be confirmed by deformation experiments conducted on forsterite-enstatite composites. Deformed composites containing a volume fraction of forsterite of less than 40% have a structure corresponding to the IWL while the forsterite-enstatite composites containing a volume fraction above 60% of forsterite show a structure akin to the LBF. In composites containing 40-60% forsterite both phases are interconnected throughout (Ji et al., 2001).

2. Methods

2.1 Sample Synthesis

Sample collection and synthesis was performed by Katrin Kraus. So were the deformation experiments described later on. For the starting material undeformed to slightly strained eclogites from the eclogite type locality Hohl in the Koralpe (Austria) were crushed below their grain size, ground and separated into garnet and omphacite. The material was again ground and sieved to grain size of 40-70 µm. The powders of the mineral fractions were mixed to obtain samples containing 25, 50 and 75 volume percent garnet. The mixed powders were uniaxially cold pressed to 30 bar into gold jackets which were mechanically sealed, resulting in samples with a height of 10 to 12 mm, a diameter of 4 mm and a wall thickness of the gold jacket of 0.2 mm. Thereafter, samples were synthesized in a piston-cylinder apparatus using sodium chloride as a confining medium, a graphite resistance furnace for heating and a NiCr-Ni thermocouple to control temperature. Synthesis conditions were set to 1100 °C and 3 GPa for 72 h. Samples remained straight and cylindrical after synthesis while the volume was reduced by up to 22%.

2.2 Deformation Experiments

Triaxial deformation experiments were performed in a servohydraulically-controlled solid-medium modified Griggs-type deformation apparatus (Fig. 3; Moghadam et al., 2010; Griggs, 1967; Rybacki et al., 1998) at confining pressures of 2.5 GPa, temperatures of 900 °C and a strain rate of $3 * 10^{-6}$ s^{-1}. All experimental work was conducted at the Experimental Geophysics Laboratory at the Ruhr-Universität Bochum (Germany). Synthesized samples were prepared to a cylindrical shape with a diameter of 3.1-3.4 mm and a height of 6.5-7.5 mm and mechanically sealed in a gold jacket (Fig. 4).

All deformed samples show a strain gradient from top to bottom whereas the bottom shows the highest degree of deformation. Estimated strain values therefor represent the average sample strain. Microstructural investigations focus on the lower half of the samples and strain is likely to be higher than the average value.

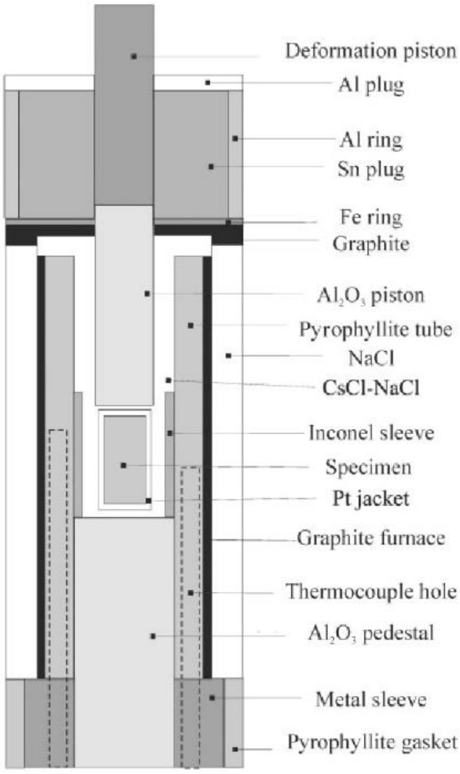

Figure 3. Sketch by Moghadam et al. (2010) of the sample assembly used for deformation tests

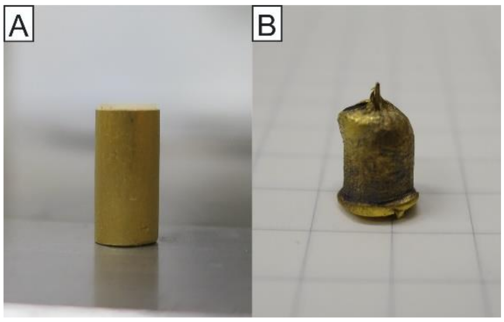

Figure 4. Sample sealed in gold jacket before (A) and after (B) deformation.

2.3 Microstructural analysis

Microstructural analysis was conducted on two samples of the starting material containing 25 and 75% garnet respectively and on three samples of the deformed material containing 25, 50 and 75% garnet to identify the active dominant deformation mechanisms, and its dependence on the phase abundance of the sample.

2.3.1 Thin Section Preparation

To prepare the thin sections, the synthetic samples were cut along their cylindrical axis and prepared into mechanically polished thin sections with a thickness of about 30 µm. For scanning electron microscopy (SEM) and electron backscatter diffraction (EBSD) analysis the thin sections were chemically polished for 3 hours with colloidal silica and coated by carbon to establish conductivity.

2.3.2 Optical Microscopy

Optical microscopy has been used for a first investigation of the microstructures and to identify potentially active deformation mechanisms. First the thin sections were scanned using a Nikon colournegative CoolscanV ED scanner to provide an initial overview of the sample and aid navigation during the applications of further methods. Optical microscopy was performed using a Leica DM4500 P microscope. The thin sections were analysed via polarized and cross-polarized light. Additionally, the lambda plate has been inserted to better identify microstructures of garnet. Reflected-light microscopy was performed to help navigation for EBSD mapping.

2.3.3 Secondary Electron Microscopy

2.3.3.1 Secondary- and Backscattered electron imaging

A FEI InspectS SEM at the Department of Geology (University of Vienna) has been used for secondary electron (SE) and backscattered electron (BSE) imaging. The SEM has been operated at an acceleration voltage of 10 kV and a spot size of 5. Overview pictures representative of the samples and detail images have been taken to document mineral distribution, possible chemical zoning, phase boundaries and microporosities. Areas of interest for further microstructural investigations have been identified.

2.3.3.2 Forward scattered electron imaging and electron backscattered diffraction mapping

In order to analyse the degree of intracrystalline plasticity forward scattered (FSD) electron imaging and EBSD mapping has been performed on a FEI Quanta 3D FEG instrument at the Department of Lithospheric Research (University of Vienna). The instrument has been operated at an acceleration voltage of 15 kV, a spot size of 1 and a sample tilt of 70° at a working distance of 14 mm.

EBSD maps were acquired with OIM Data Collection Software at step sizes between 0.33 and 0.7 µm. The EBSD data have been processed using the TSL OIM Analysis software. The data was cleaned according to a Confidence Index (CI) <0.1, CI standardization up to cleanup level 1 and neighbor orientation correlation up to cleanup level 1. The grain tolerance angle was set to 10° and the minimum grain size to 3 pixels.

Color coded invers pole figure, grain average misorientation-, aspect ratio, orientation deviation – angle maps were plotted, as well as grain size (equivalent diameter)-, grain average misorientation- and aspect ratio charts and axis/angle misorientation distribution function plots. The aspect ratio is calculated as the length of the minor axis divided by the length of the major axis, with the major axis being the maximum distance between the endpoints of each boundary segment, and the minor axis being calculated with an averaging scheme. In orientation deviation – angle maps each point is shaded according to its angular deviation to the average orientation for the grain to which it belongs. For grain size charts the diameter of a particular grain is calculated by determining the area (A) of a grain and then assuming the grain is a circle. The diameter (d) is then calculated using the following equation:

$$d = 2\sqrt{\mathrm{A}/\pi} \qquad \text{(Eq. 1)}$$

Stereographic projections of (001), (010) and (100) poles of omphacite and [001], [011] and [111] axis of garnet have been plotted as equal angle and upper hemisphere projections. Maps and charts were created for garnet and omphacite respectively. For omphacite, new partitions for grain sizes of 5-10 µm and 10-100 µm were made. Invers pole figure maps, pole figure plots and axis/angle MDF plots were created for those partitions.

Grain Files including information about area in square µm, diameter in µm, aspect ratio, ellipse major axis in µm, orientation of major axis relative to horizontal, orientation spread in degrees and average misorientation were exported for omphacite and garnet and further processed in Excel. Previous to processing, data have been cleaned by eliminating grains smaller than 3 pixels and grains touching scan edges. Mean, mode and standard deviation were determined for grain size, as well as the means of average misorientation and aspect ratio.

2.3.4 Mechanical Data

The mechanical data were acquired by Katrin Kraus. The differential stress was determined by correcting the measured load for dynamic friction and division by the initial cross-sectional area. The uncertainty for the derived stress is conservatively estimated to ±0.2 GPa (Druiventak et al., 2011). The axial strain is derived by correcting the displacement for stiffness of the apparatus considering the initial length of the sample. All strain values are given as natural strain in percentage, the natural logarithm of the engineering strain added one ($\varepsilon = \ln(e + 1)$). The uncertainty in the derived strain is estimated to 0.1% accounting for the accuracy of the displacement transducer and the uncertainty of the stiffness correction (Moghadam, 2010). Differential stress was plotted against strain in Excel and the maximum differential stress was determined.

3. Results

The following section is focusing on results from microstructural investigations using, optical microscopy, SE-, BSE-, and FSD imaging as well as EBSD mapping. Prior to results from the three deformed eclogite samples, the microstructure of undeformed synthesized eclogite containing 25 and 75% garnet will be presented for reference. Microstructures of deformed samples are presented separately with respect to garnet content of samples. Additionally, mechanical data conducted during the deformation experiments are shown.

3.1 Starting Material

3.1.1 Microstructure

Omphacite-Garnet aggregates containing 25% volume fraction of garnet are characterized by a nearly random fabric comprised of garnet clusters of varying orientation surrounded by an omphacite matrix (Fig. 5). The garnet clusters usually consist of a few larger grains of around 20 to 50 µm, surrounded by smaller garnet grains of a few micrometres (Fig. 5B). In general garnet grains have a maximum size of 100 µm and are characterized by straight to slightly curved grain boundaries. The average aspect ratio calculated from EBSD maps is 0.53 and the average diameter is about 8 µm. Minor porosity occurs within and surrounding the garnet clusters (Fig. 6). Omphacite shows a large variation in grain size ranging between a few micrometres up to 200 µm. Areas of grains with a diameter of even less than one micrometre are found along omphacite-garnet phase boundaries and occasionally surrounding larger omphacite grains (Fig. 5B). The average diameter of omphacite determined from EBSD maps is 5.81 µm with an average aspect ratio of 0.51. Omphacite grains show both, straight and rounded grain boundaries and often exhibit undulatory extinction. Deformation twins are observed only rarely. Both, garnet and omphacite show horizontal micro-cracks which are interpreted as decompression fractures. Locally, those decompression fractures run through the entire thin section (Fig. 5A).

Omphacite and garnet often show a chemical zoning indicated by a grey shade variation in BSE images (Fig. 6A, B). Omphacite exhibit lighter rims which are associated with minor iron enrichment and depletion in magnesium (Fig. 6A) whereas darker garnet rims are enriched in iron and depleted in magnesium (Fig. 6B). Similar grey shade variation can be observed along micro cracks or more randomly in garnet located in cluster (Fig. 6A, B).

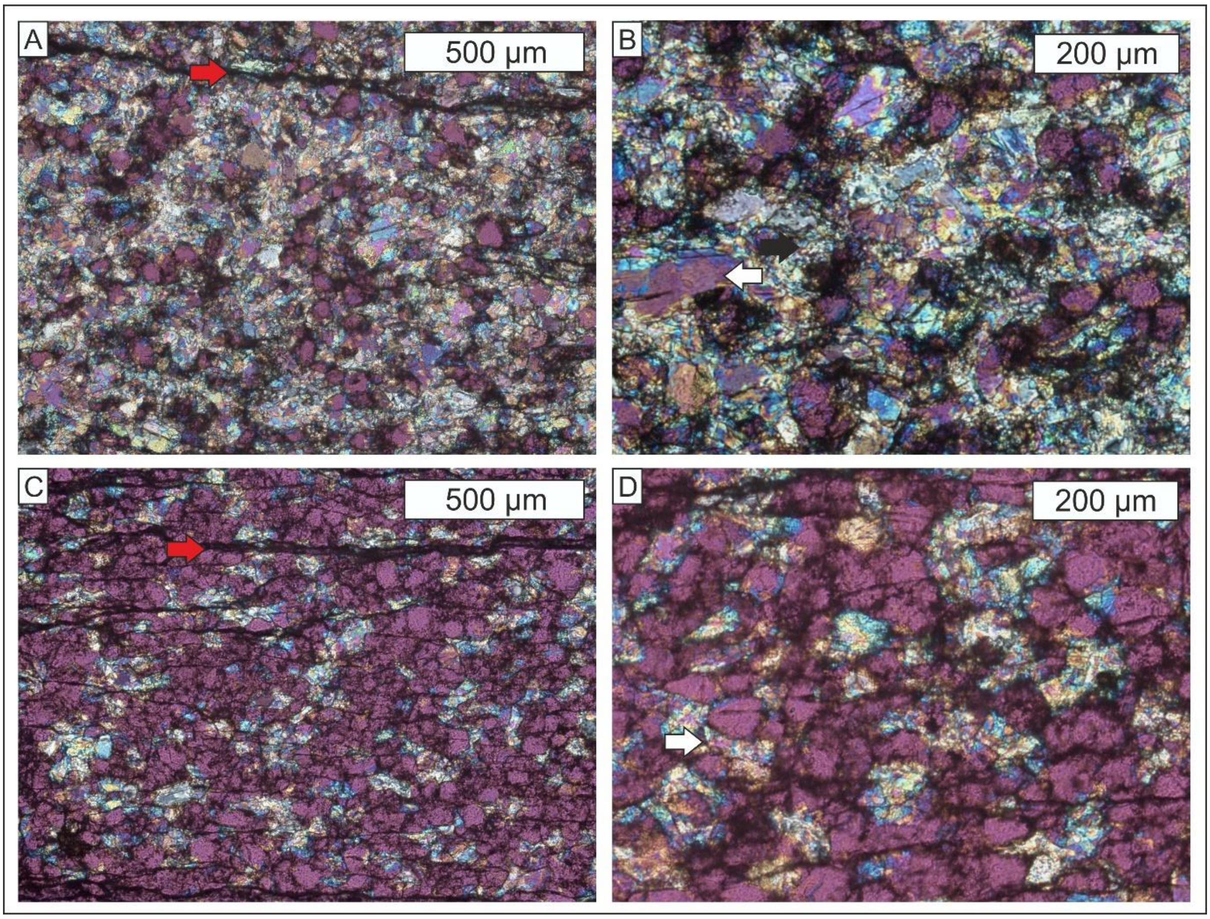

Figure 5. Optical microscope images of synthesized eclogite containing a 25% volume fraction (A, B) and 75% volume fraction of garnet (C, D). Crossed polarizers and lambda plate inserted. A) Nearly random fabric with garnet grains and cluster in an omphacite matrix. Red arrow points to decompression crack. B) Omphacite grains are partly elongated and show undulatory extinction (white arrow). Locally subgrains occur (black arrow). C) Interconnected garnet matrix with randomly distributed omphacite cluster. Red arrow points to decompression cracks. D) Locally omphacite is squeezed between garnet (white arrow).

The starting material containing 75% volume fraction of garnet is characterized by interconnected framework of garnet surrounding omphacite clusters (Fig. 5C, D). In omphacite rich areas garnet tends to form layers with a somewhat horizontal orientation defining a slight foliation (Fig. 5C). Horizontal decompression cracks are common and often cross a large portion if not the entire thin section (Fig. 5C). Especially garnet is characterized by a high density of horizontal cracks while omphacite seems to be less affected. Garnet shows grainsizes of up to 100 µm. Smaller garnet grains of a few micrometres are often found in aggregates between larger grains. Garnet has mostly rounded grain boundaries. The average diameter of garnet in the EBSD map is 3.90 µm and the average aspect ratio is 0.53. Omphacite has grainsizes of up to 100 µm and mostly curved grain boundaries. Omphacite clusters consist of a combination of larger grains and small grains of a few micrometres, or just small grains. Larger omphacite grains often show an elongation. Their orientation is dependent on the surrounding garnet. The average aspect ratio of omphacite detected in EBSD maps is 0.51 and the average diameter is 3.91 µm. Again, omphacite grains exhibit undulatory extinction and rarely twinning.

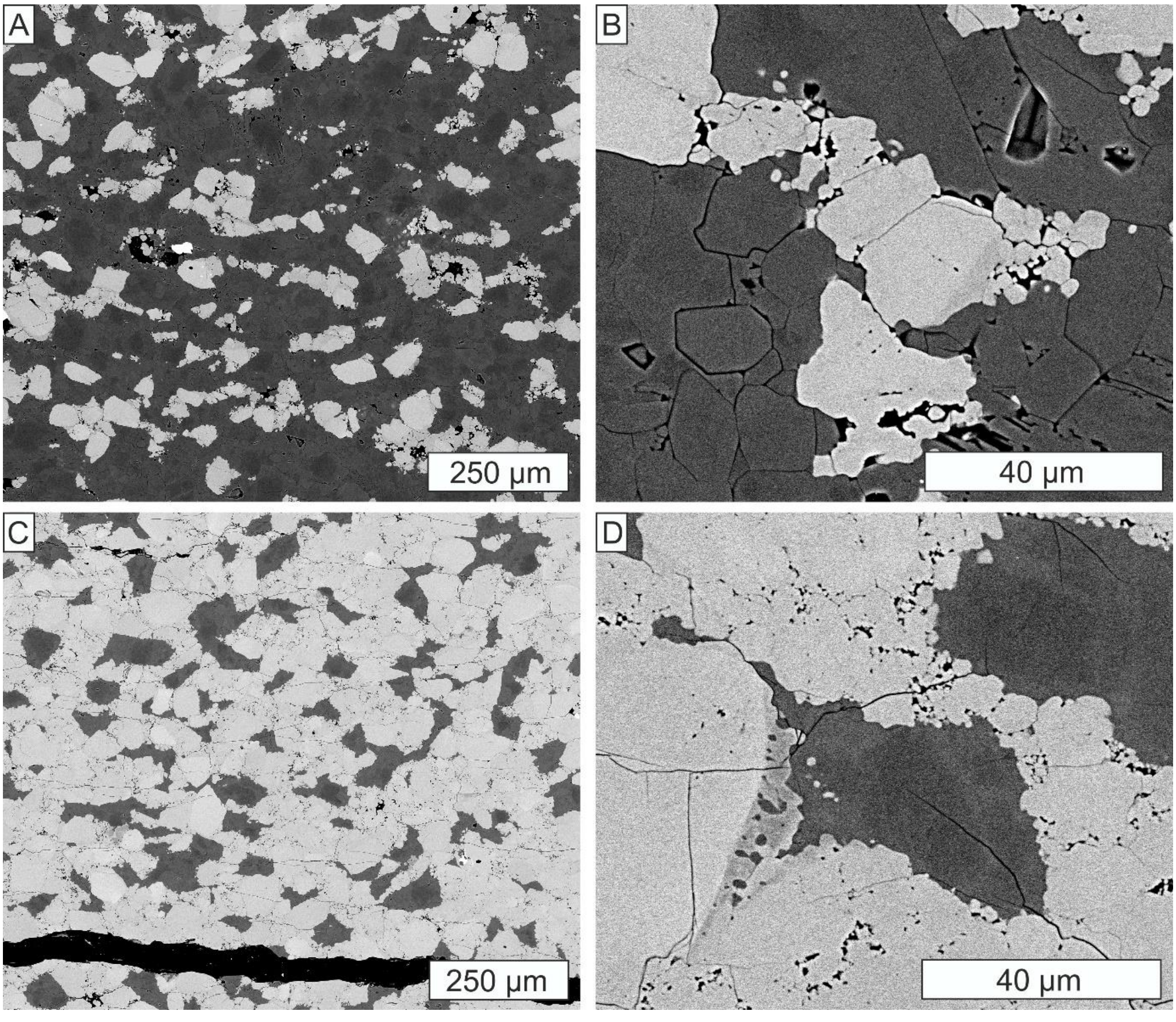

Figure 6. Backscattered electron images of synthesized eclogite containing a 25% volume fraction (A, B) and 75% volume fraction of garnet (C, D). A) Locally elongated garnet cluster, minor chemical zoning in omphacite with lighter rims and darker cores, micro-porosity often at garnet cluster. B) Straight omphacite grain boundaries, micro-porosity, fragmented garnet cluster with < 10 µm size and slightly darker in colour. C) Interconnected garnet fabric, random omphacite distribution, decompression cracks. D) Garnet overgrowth, fragmented garnet.

In the BSE images chemical zoning can be seen. Omphacite rims are often enriched in iron and depleted in magnesium. Garnet shows grain sizes of up to 100 µm. The average diameter of garnet in the EBSD map is 3.90 µm and the average aspect ratio is 0.53. Garnet grains are mostly circular to slightly elongated with straight to slightly curved grain boundaries. In the BSE images Garnet again exhibits chemical zoning, mainly towards the rim of the grain but also more randomly. Rims are enriched in iron and depleted in magnesium (Fig. 6D).

3.1.2 Intracrystalline plasticity

In both samples of the starting material omphacite has a weak crystallographic preferred orientation (CPO). Pole figures of omphacite show a preferred alignment of (001) poles along a girdle within the foliation while poles to (010) show a weak maximum perpendicular to the foliation (Fig. 7).

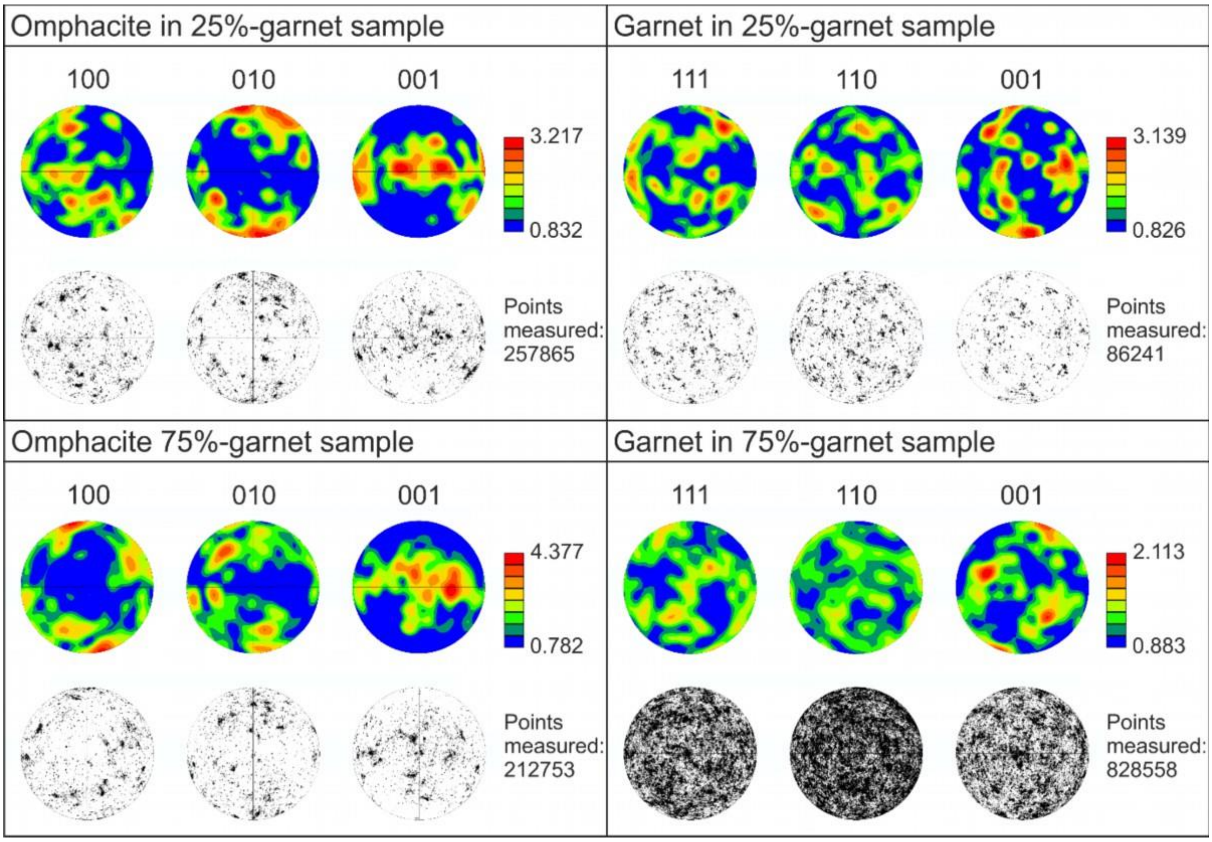

Figure 7. Stereographic projection of poles to the (100), (010) and (001) planes of omphacite and <111>, <110> and <001> axis of garnet. Upper hemisphere and equal area projection contoured according to the orientation distribution function (top) and uncontoured (bottom). Details can be found in the text (section 3.1.2)

The poles to (100) show a varying orientation with garnet content in the samples and are either aligned preferentially along the periphery of the pole figure (75% garnet sample) or show a close to random orientation (25% garnet sample; Fig. 7). Misorientation axis plotted in inverse pole figure space show a weak maximum around [001] for small misorientations (Fig. 8).

Omphacite does not show areas indicative of strain localisation in the EBSD maps (Fig. 9) in accordance with an average misorientation below 1. Still, minor signs of intracrystalline deformation are present. Low-angle grain boundaries can be observed in the vicinity of cracks (Fig. 9A, C). Pole figure plots of garnet of both samples show local point maxima, however, the distribution is quite random (Fig. 7). In the misorientation axis plots no maxima are apparent (Fig. 8).

Garnet shows some signs of plastic deformation in the form of misorientation, though they tend to be minimal in larger grains (Fig. 9B, D). Higher misorientation deviations tend to occur in smaller grains. The average misorientation of garnet is minimal increasing with garnet content in the sample. However, with an average of 0.56 (25% garnet sample) and 0.69 (75% garnet sample) it is extremely low. Low-angle grain boundaries are found mostly around cracks. It should be noted that several low-angle grain boundaries detected by EBSD actually represent micro-cracks.

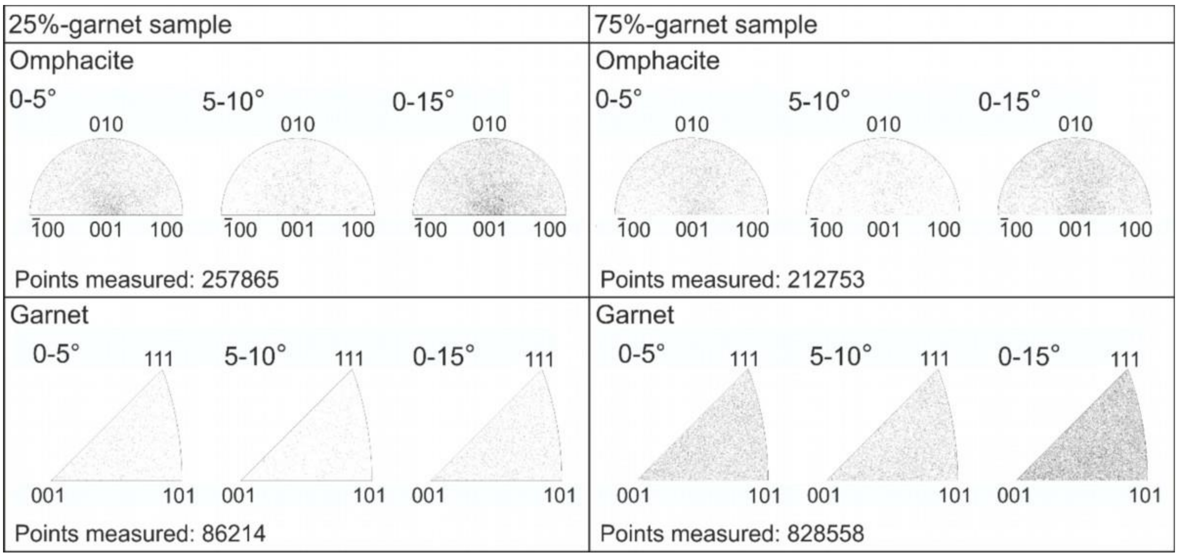

Figure 8. Inverse pole figure plots of rotation axis for misorientation angles between 0-5°, 5-10° and 0-15° of omphacite and garnet from samples containing a 25% volume fraction (left) and 75% volume fraction (right) of garnet. Plots of omphacite of the 25% garnet sample show a maximum at 001. Both plots of garnet show no maximum.

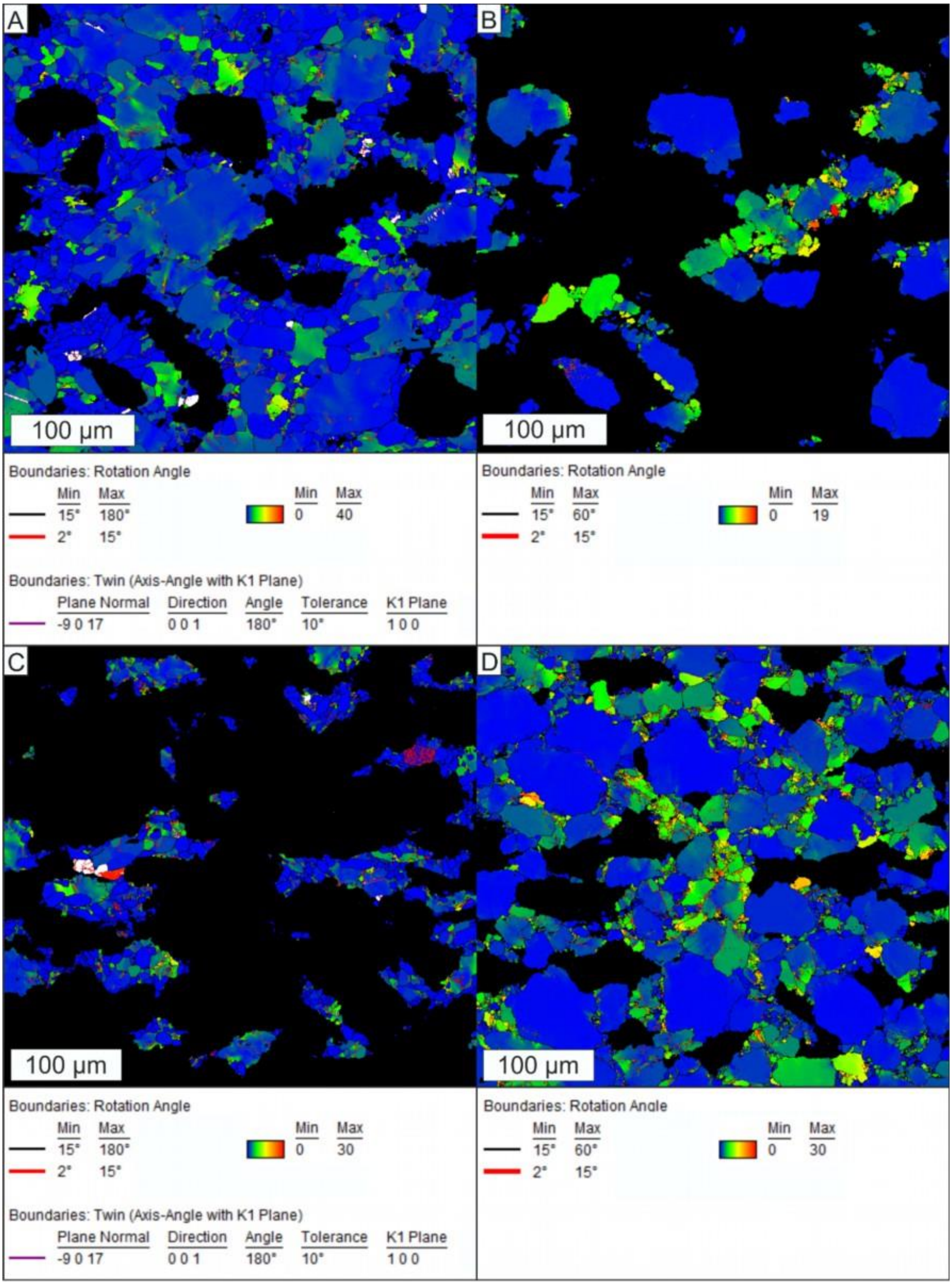

Figure 9. Misorientation deviation angle map of the deformed eclogite containing a 25% (A,B) and 75% (C,D) volume fraction of garnet. Low-angle (<15°) grain boundaries are in red, grain boundaries (>15°) in black and twins in omphacite are in purple. A,C) In omphacite low-angle grain boundaries tend to appear around cracks B,D) In garnet higher misorientation deviation angles tend occur in smaller grains.

3.2 Deformed Samples

3.2.1 Mechanical Data

Mechanical data conducted during deformation experiments show that the strength of eclogite is varying with garnet content in the sample. The differential stress against strain plots (Fig. 10) indicate a different rheological behaviour for all three samples. For the deformed eclogite containing a 25% volume fraction of garnet the plot of differential stress (GPa) against strain shows, that from a strain of 0 to 6, the stress increases. Maximum stress of around 0.76 GPa is reached at 6.5% strain and after that slowly decreases again. At a strain of 18%, stress has gone back down to 0.84 GPa. For the 50% garnet sample, from a strain of 0 to about 5.5% stress increases to around 0.96 GPa. After 5.5% stress increases only slightly and reaches the maximum of about 1.02 GPa at a strain of 6.8%. After that the stress decreases at first slightly and after about 7.3 more significantly. For the 75% garnet sample stress increases somewhat steadily until a strain of about 8. From 8% onwards stress increases less and less. At a strain of 12.37% the maximum stress of around 1.07 GPa is reached. After that stress decreases. Overall, two main characteristic changes can be observed in the rheological behaviour of eclogite with increasing garnet content in the sample:

- The maximal differential stress is increasing with increasing garnet content. Especially between the 25%- and 50%-garnet sample a drastic jump can be observed.
- The maximal differential stress is reached at higher strain with increasing garnet content.

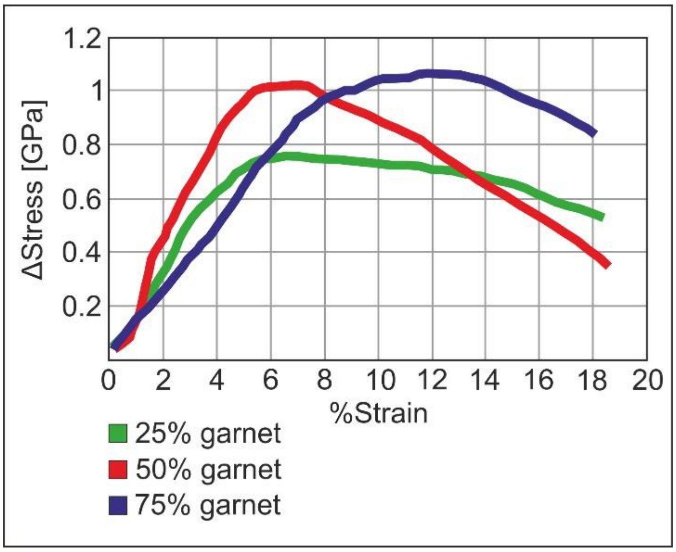

Figure 10. Differential stress plotted against strain.

3.2.2 25% Garnet Sample

3.2.2.1 Microstructure

The deformed sample containing a 25% volume fraction of garnet is defined by a weak foliation which is characterized by a shape preferred orientation (SPO) of omphacite and horizontal to sub-horizontal garnet layers (Fig. 11A). Theses garnet layers are made up of both more circular grains arranged in garnet chains, as well as elongated grains with a foliation-parallel SPO. Such elongated garnet aggregates never run through the entire thin section and rarely exceed 500 µm in horizontal length. Single garnet grains surrounded by omphacite can be observed frequently.

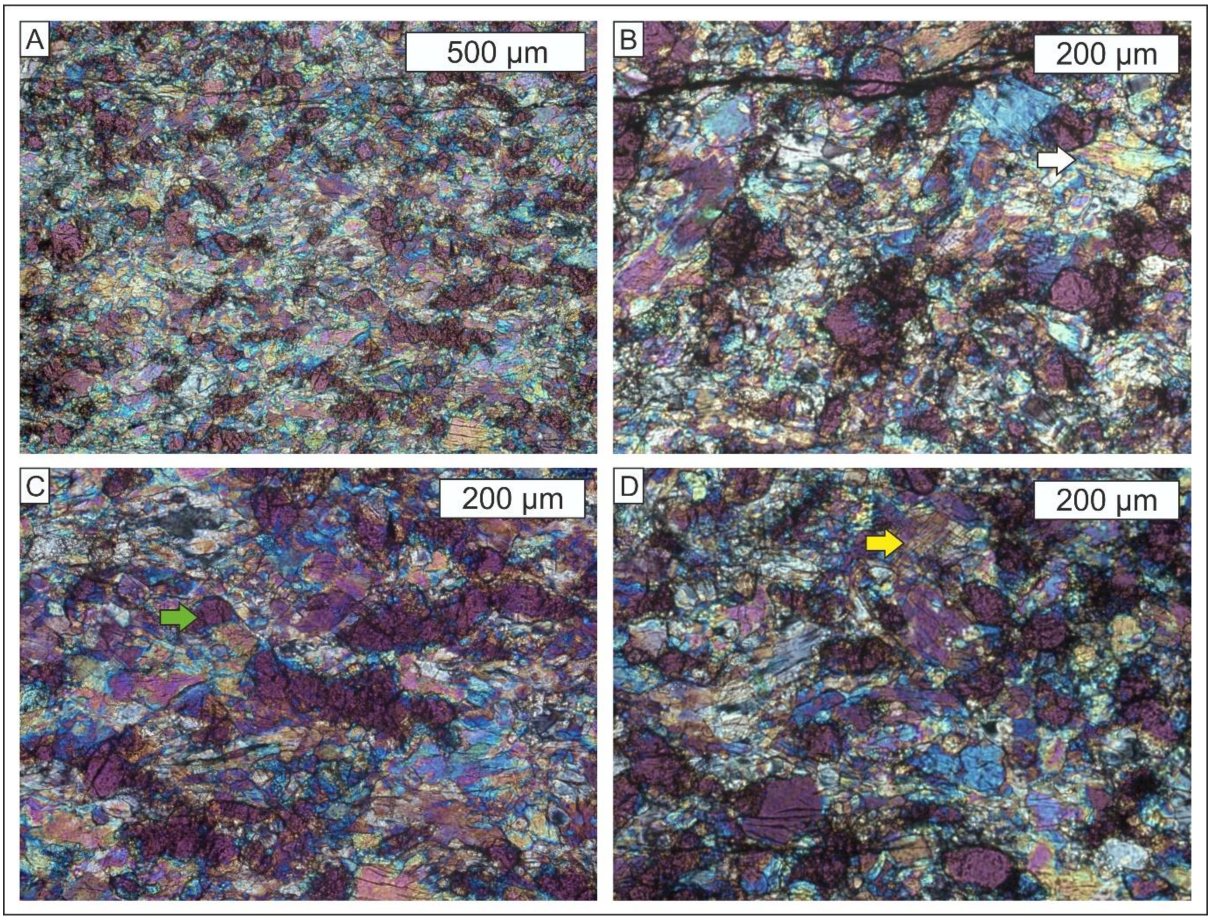

Figure 11. Optical microscope images of deformed eclogite containing a 25% volume fraction of garnet. Crossed polarizers and lambda plate inserted. A) Garnet occurs in both random clusters and horizontal layers in an omphacite matrix. B) Omphacite shows great differences in grainsize. Omphacite grains are often elongated and show undulatory extinction (white arrow) C) Garnet forms horizontal layers in an omphacite matrix and commonly shows vertical cracks (green arrow). D) Larger Omphacite grains often show twinning (yellow arrow).

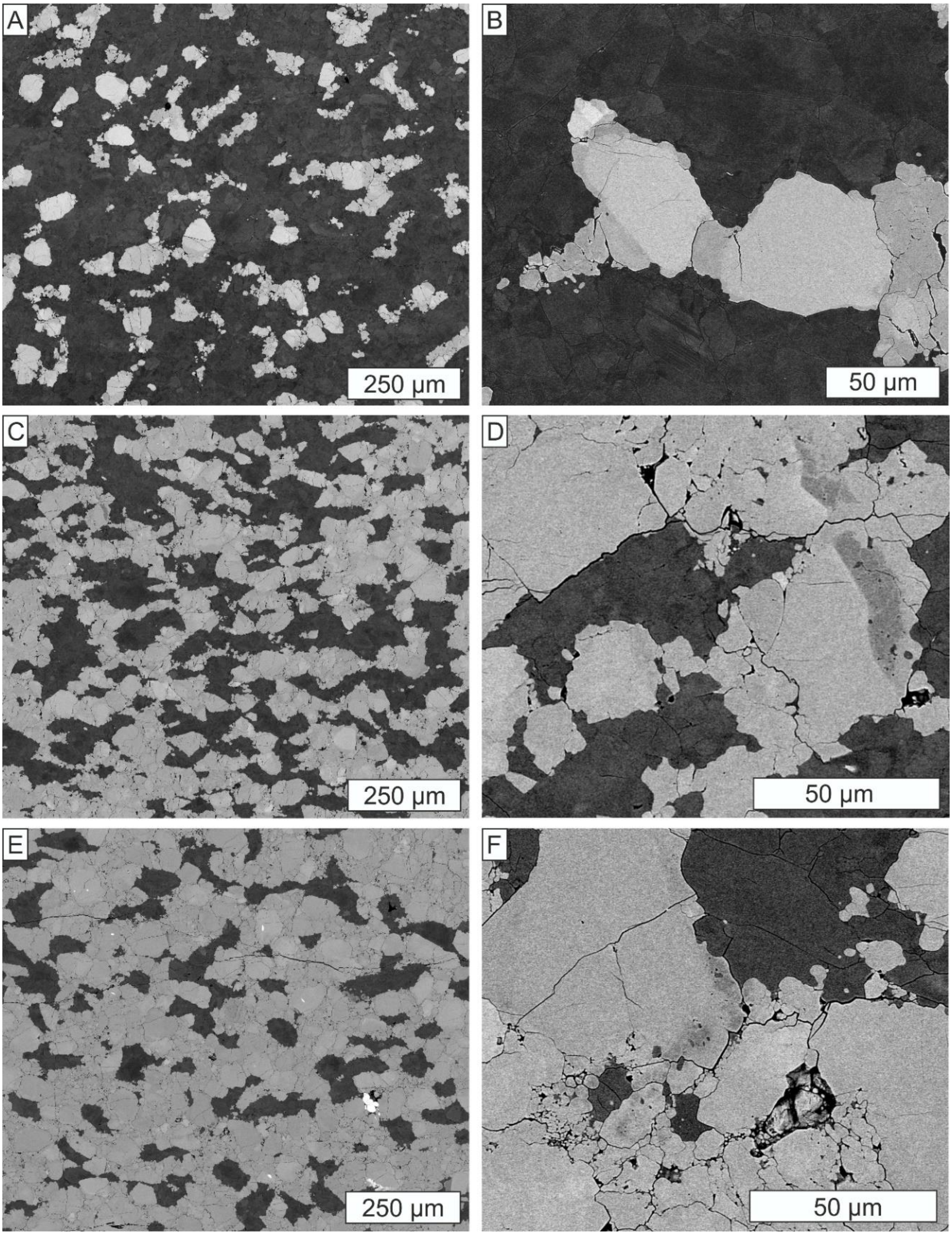

Figure 12. Backscattered electron images of deformed eclogite containing a 25% volume fraction (A, B), 50% volume fraction (C, D) and 75% volume fraction of garnet (E, F). A) Garnet clusters in an omphacite matrix, chemical zoning in garnet and undulatory extinction in omphacite. B) Chemical zoning in garnet, twins and undulatory extinction of omphacite. C) Interconnected garnet layers, undulatory extinction and some chemical zoning of omphacite, micro-porosity. D) Fragmented garnet, overgrowth of garnet, micro-porosity. E) Interconnected garnet fabric, random omphacite distribution. F) Fragmented garnet, overgrowth of garnet, micro-porosity.

Garnet grains show diameters of a few micrometres to 100 µm with mostly rounded or angular grain boundaries. Often garnet grains of a few micrometres are found between larger garnet grains. The average aspect ratio of garnet in the overview map is 0.53 and the average diameter is 5.08 µm. Garnet fractures often resemble intragranular cracks which cut through the entire garnet grain without continuing into the adjacent omphacite grains. Fractures are also often perpendicular to the foliation (Fig. 11C). BSE imaging of garnet again reveals chemical zoning, with darker rims indicating a depletion in iron and enrichment in magnesium (Fig. 12A, B).

Larger omphacite clasts are often elongated and form a foliation parallel SPO. Smaller omphacite grains of a few micrometres are often accumulated around garnet grains or larger omphacite grains. This sample omphacite shows grain sizes of a few micrometres to up to 200 µm. Omphacite grain boundaries are often curved, especially in larger grains. Grains of around 50 µm and smaller may show straighter grain boundaries. The average aspect ratio of omphacite in the overview EBSD map is 0.47 and the average diameter is 4.93 µm. Most omphacite grains show undulatory extinction. Twins are very common (Fig. 11D), especially in larger grains with diameters of 100 µm and above. Both undulatory extinction and twins are also visible in the BSE images (Fig. 12A, B). Fractures in Omphacite occur in all directions. Within larger grains they are sometimes parallel to the foliation and distributed somewhat evenly.

3.2.2.2 Intracrystalline plasticity

Pole figure plots show that omphacite developed a CPO with (010) poles perpendicular to the foliation while poles to (001) form a slightly dispersed girdle within the foliation with maxima parallel to the horizontal axis of plots (Fig. 13). When comparing pole figures of clast larger than 10 µm with those for grains smaller than 10 µm, one notices that poles to (001) in larger clasts form strong point maxima (~16.5 ODF) parallel to the pole figure horizontal whereas in smaller grains a girdle can be observed (Fig. 13). The misorientation axis plots reveal a maximum parallel to [001] (Fig. 14). Pole figure plots of garnet show several dispersed point maxima, however those are orientated randomly and are quite weak (~2.7 ODF; Fig. 15).

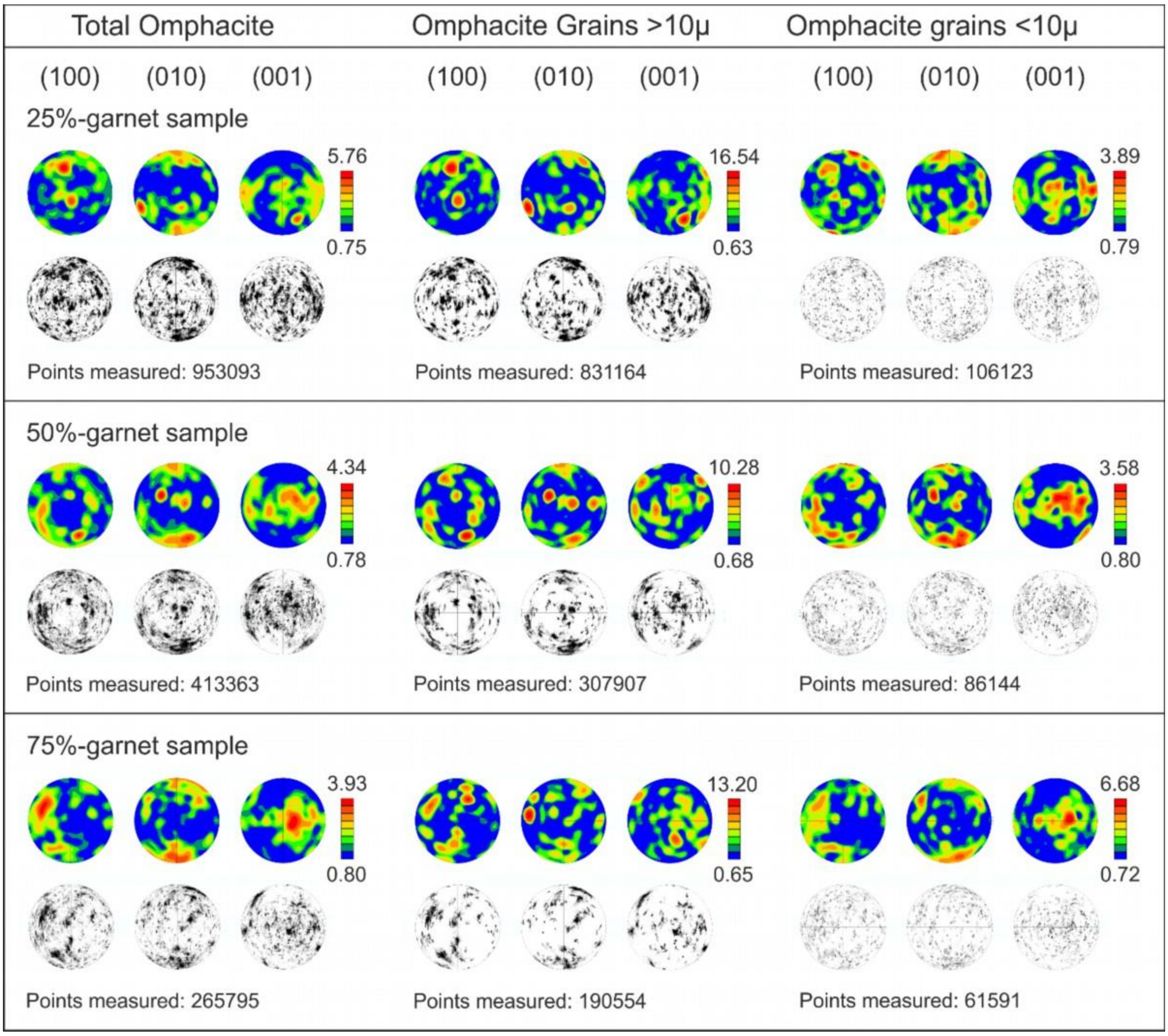

Figure 13. Stereographic projection of poles to the (100), (010) and (001) planes of omphacite. Upper hemisphere and equal area projection contoured according to the orientation distribution function (top) and uncontoured (bottom). Details can be found in the text (section 3.2.2.2, 3.2.3.2, 3.2.4.2)

In accordance to the random crystallographic orientation axis plots do not show any maxima (Fig. 16). Omphacite shows recrystallisation near phase boundaries. Low-angle grain boundaries occur more often than in the starting material, both around cracks as well as in the centre of grains. Planar features which will be further discussed below (**3.2.2.3 Trace analysis**) are commonly found. Grains showing little to no misorientation are usually smaller. The average misorientation of omphacite in the EBSD map (Fig. 17A) is 1.16, slightly higher than the starting material.

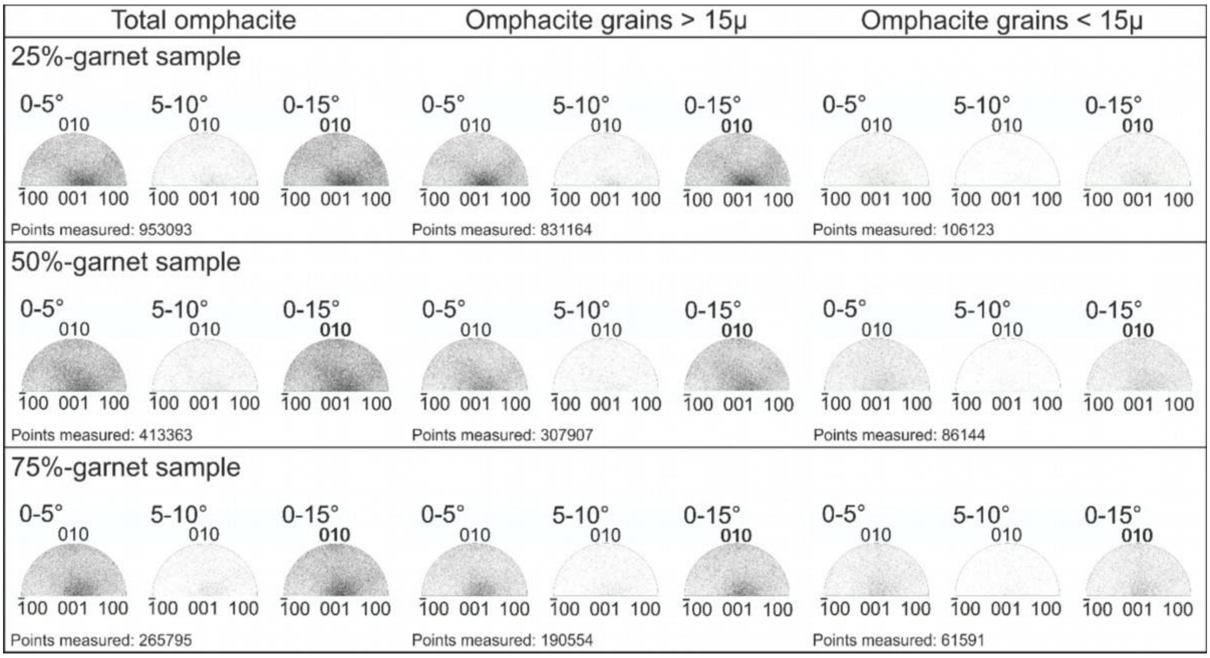

Figure 14. Inverse pole figure plots of rotation axis for misorientation angles between 0-5°, 5-10° and 0-15° of omphacite from samples containing a 25% volume fraction, 50% volume fraction and 75% volume fraction of garnet (from top to bottom). Rotation axis are further plotted separately for grain size fractions of >15 µm and <15 µm. For all samples the plots show a maximum at 001, which is more noticeable for angles between 0-5°.

Similar to omphacite, we observe brittle and crystal plastic deformation features in garnet. Low angle grain boundaries occur mostly along cracks but can also be observed independently. In areas where Garnet shows higher misorientations, the surrounding omphacite is often also characterized by higher degrees of misorientation and a higher density in low-angle grain boundaries and/or recrystallisation. The average misorientation of garnet in the EBSD map is 0.64 (Fig. 17B).

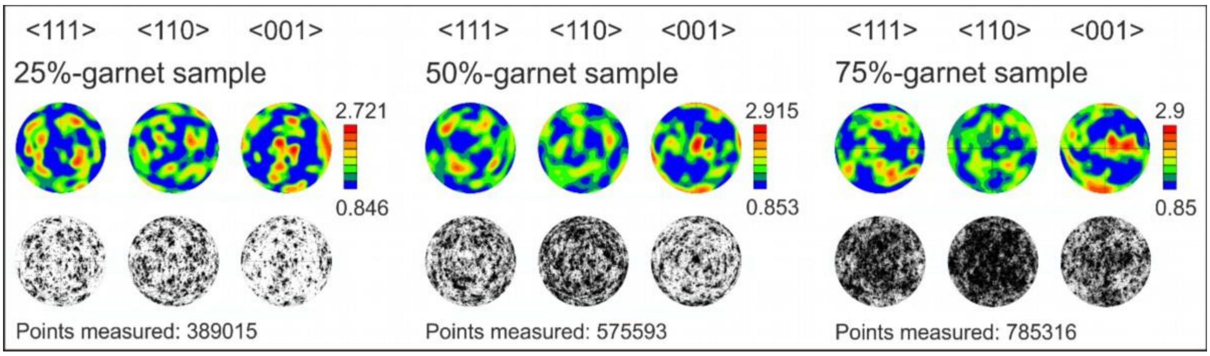

Figure 15. Stereographic projection of poles to the <111>, <110> and <001> axis of garnet. Upper hemisphere and equal area projection contoured according to the orientation distribution function (top) and uncontoured (bottom). Details can be found in the text (section 3.2.2.2, 3.2.3.2, 3.2.4.2)

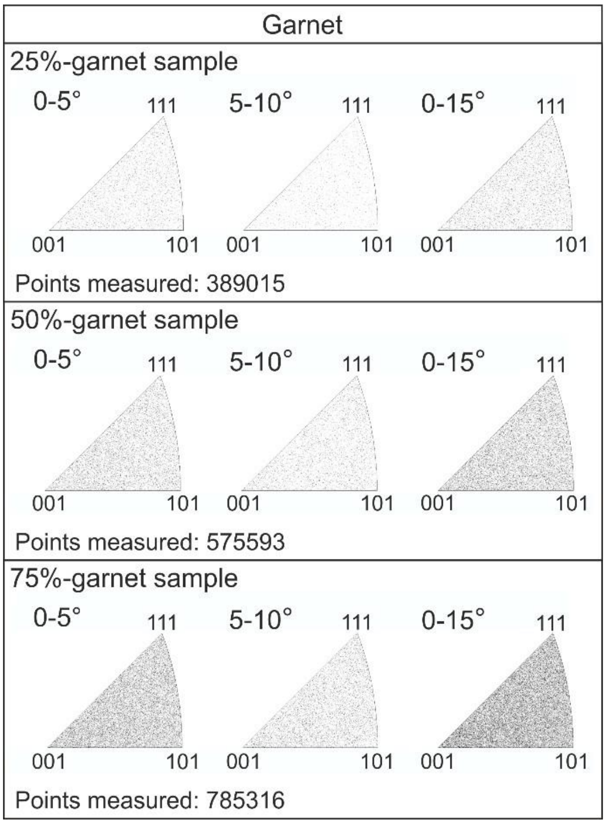

Figure 16. Inverse pole figure plots of rotation axis for misorientation angles between 0-5°, 5-10° and 0-15° of garnet from samples containing a 25% volume fraction, 50% volume fraction and 75% volume fraction of garnet (from top to bottom). For all samples the plots show no maximum.

3.2.2.3 Trace analysis of planar features

In several EBSD maps omphacite clasts show distinct planar features with either increased misorientation or offsetting misorientations (Fig. 18). Some clasts show a variety of plane traces crosscutting each other. To check whether these features represent slip lines, cleavage planes or twins I analysed their traces and misorientation characteristics. The deformed omphacite-garnet aggregate containing 25% volume fraction of garnet the omphacite contains planar features which follow the (100) plane and typically show misorientation changes of 180° perpendicular to the plane traces. Further planar features which show sudden misorientation changes of a few degrees perpendicular to them are found as well. These features appear as straight lines as well as irregular lamellae and most commonly occur along (100) and (110) planes. Some match the (010) and (001) planes as well. Misorientation profiles parallel to planar features usually show a gradual in- and decrease in misorientation.

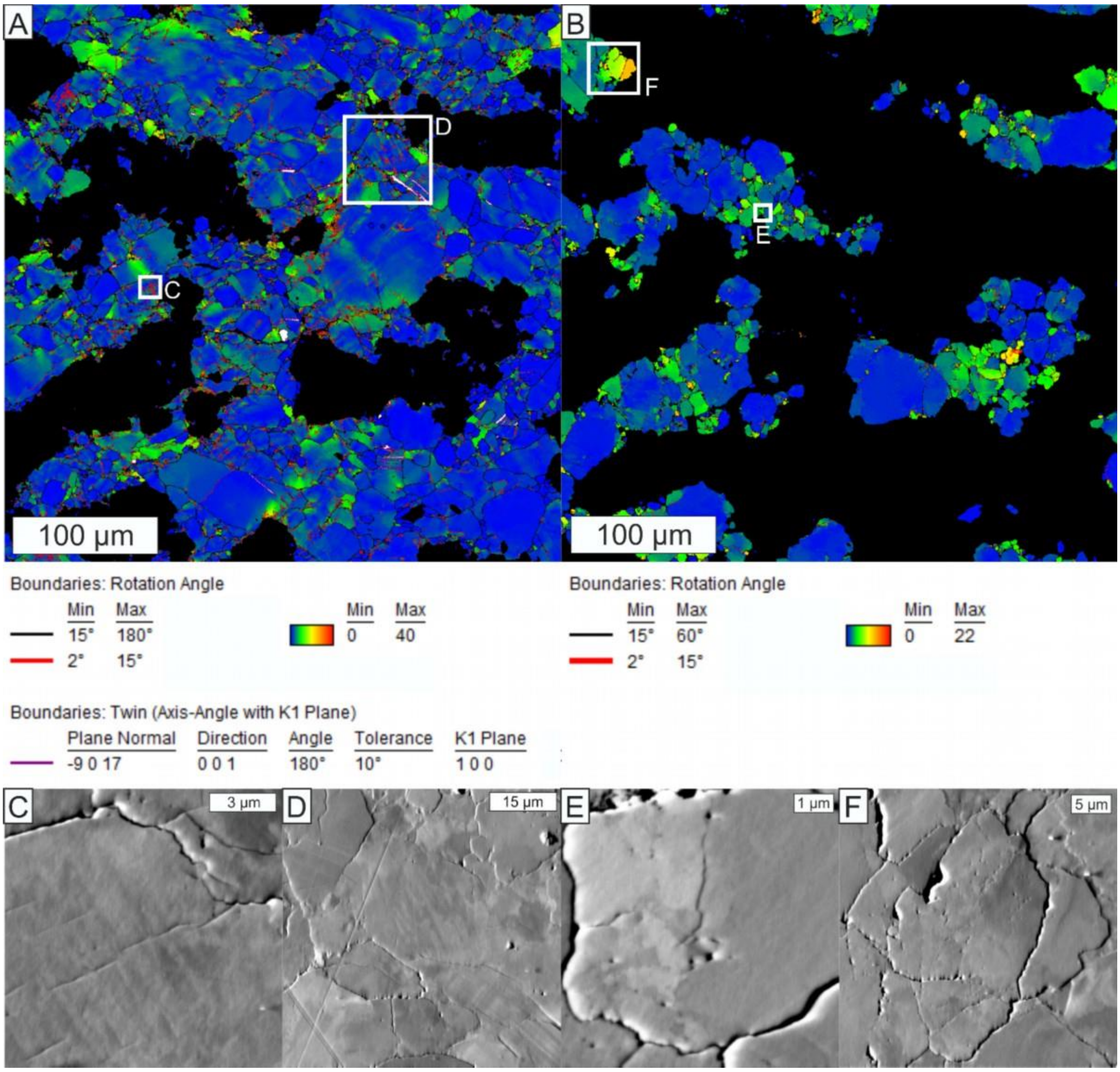

Figure 17. Misorientation deviation angle map of the deformed eclogite containing a 25% volume fraction of garnet. Low-angle (<15°) grain boundaries are in red, grain boundaries (>15°) in black and twins in omphacite are in purple. Inserted rectangles mark the locality of orientation contrast images C to F. A) Smaller grainsizes of Omphacite commonly occur at phase boundaries, so do higher misorientation deviation angles and low-angle grain boundaries. Larger omphacite clasts show linear features subparallel to the misorientation pattern. B) Larger garnet clasts show a low deviation angle while smaller grains tend to be higher strained. C) Linear feature in omphacite crosscut by cracks. D) Twins and linear features in omphacite. E) Irregular orientation contrast in garnet. F) Irregular orientation contrast and linear features in garnet.

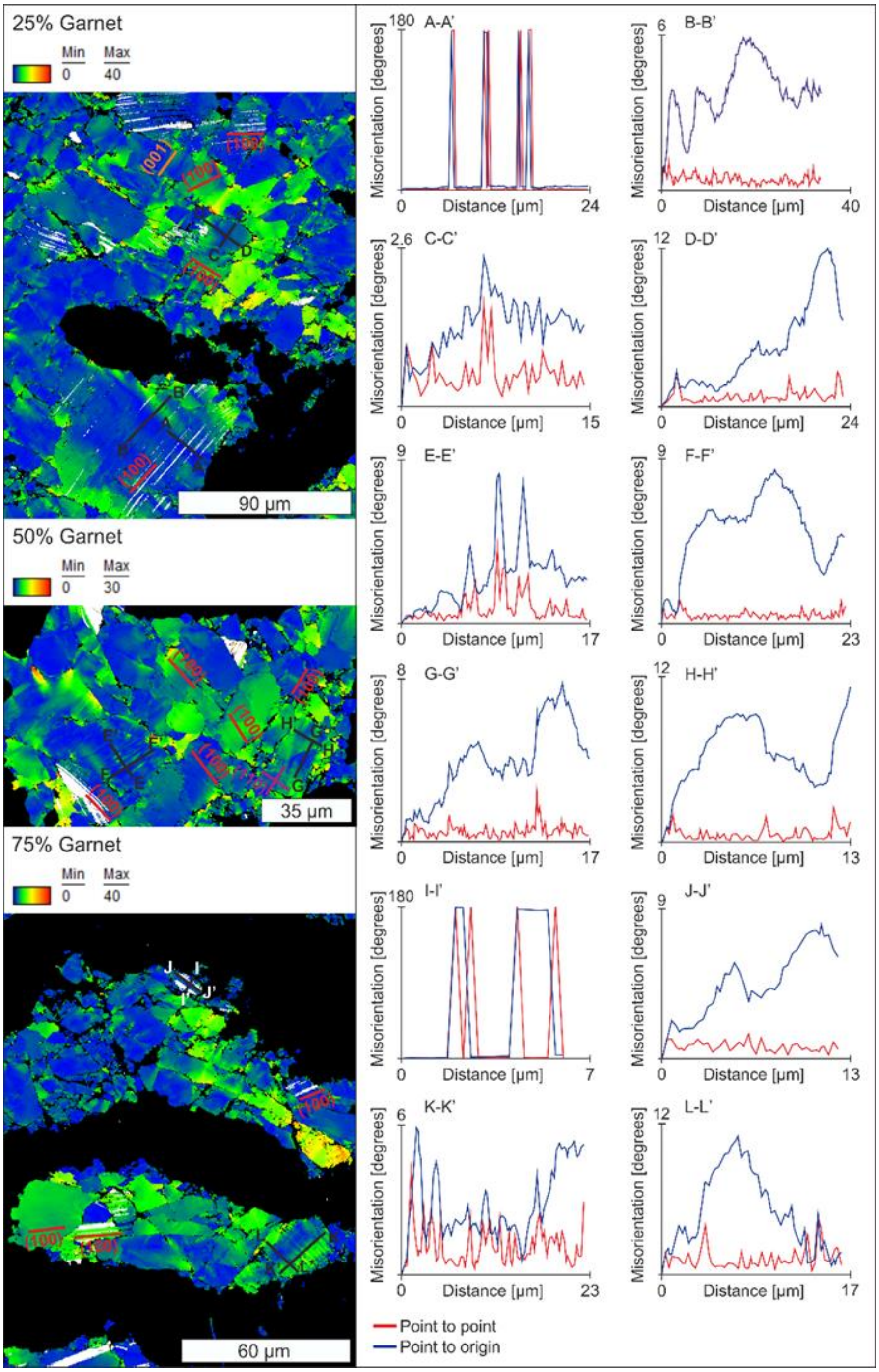

Figure 18. Misorientation deviation angle maps of omphacite from deformed eclogite with varying garnet fraction (increasing from top to bottom). Red lines indicate the trace of (100) planes, orange lines the trace (001) planes, and purple lines the trace of (110) planes. Black lines mark the locations of the misorientation profiles. A), I) Profiles across omphacite twins showing misorientations of around 180°. C), E), G), K) Profiles across slip lines show sudden changes in misorientation and misorientations of up to 8° from origin (E). B), J) Misorientation Profiles parallel to twins show more gradual in- and decreases in misorientation, with misorientation angles of up to 8° (J) form origin. The misorientation angles from point to point are under 4°. D), F), H), L) Misorientation profiles parallel to slip lines also show more gradual in- and decreases in misorientation, with misorientation angles of up to 12° (H) form origin. The misorientation angles from point to point are mostly under 4° (except for L).

3.2.3 50% Garnet Sample

3.2.3.1 Microstructure

The deformed sample containing a 50% volume fraction of garnet has a very distinct foliation (Fig. 19A). It is mainly defined by horizontal garnet layers, though their orientation varies and can deviate up to ±10° from the horizontal. These layers are made up of larger grains positioned next to each other with fine grained garnet between them. The garnet layers are often interconnected. Single grains solely surrounded by omphacite are rare. Garnet grains vary between a few micrometres to around 80 µm in diameter. Grain boundaries are mostly curved. More circular grains are still present, but elongated grains are more common.

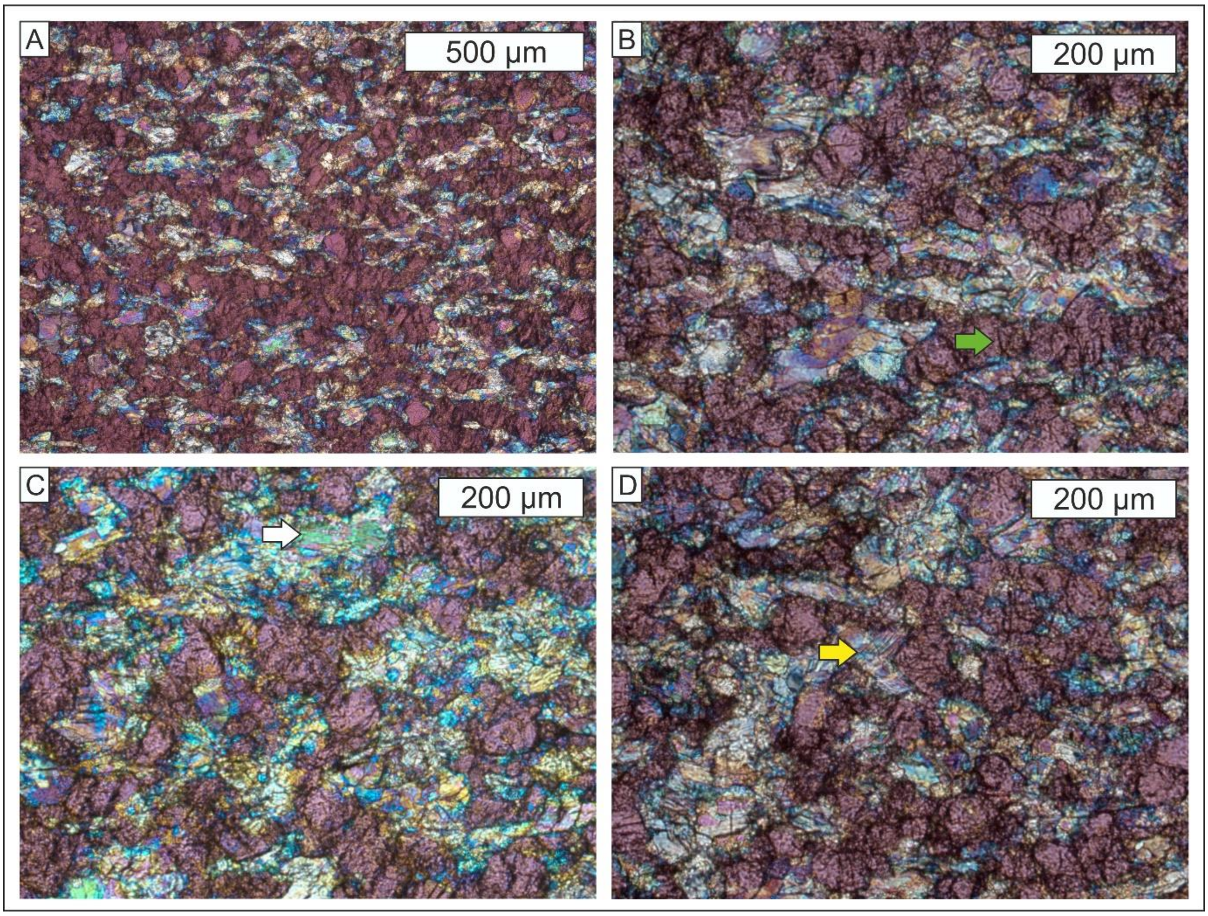

Figure 19. Optical microscope images of deformed eclogite containing a 50% volume fraction of garnet. Crossed polarizers and lambda plate inserted. A) A horizontal foliation defined by horizontal garnet layers. B) Garnet breaks more randomly, but vertical fractures still occur (green arrow). C) Omphacite grains are partly elongated horizontally and often show undulatory extinction (white arrow). D) Twins are found in larger omphacite grains (yellow arrow).

The average diameter of garnet in the EBSD map is 3.35 µm and the average aspect ratio is 0.47. Fracturing occurs more often than in the 25% garnet sample and in all directions. While there still are garnet grains breaking vertically (Fig. 19B), the orientation of fractures is more random. Garnet again shows chemical zoning towards the edge of the grain in the BSE images as well as growth rims, which appear locally as much darker areas, rather than even rims surrounding the entire grain. (Fig. 12C, D). Omphacite mostly occurs in interconnected layers between garnet layers. Larger Omphacite grains are often elongated and form a SPO which is somewhat horizontal, though their orientation can vary depending on the space they have between the surrounding garnet grains. Larger omphacite grains with no significant elongation occur in areas with less garnet present. Omphacite grains again are between a few micrometres and 100 µm in diameter and have mostly rounded grain boundaries. The average diameter of omphacite in the EBSD map is 3.27 µm and the average aspect ratio is 0.49. Twins are common, though not as abundant as in the 25% garnet sample and most grains show undulatory extinction. Undulatory extinction is also visible in the BSE images (Fig. 12D). Fracturing of omphacite also occurs more often than in the 25% garnet sample and in all directions. Parallel fractures in omphacite like in the 25% garnet sample are rare.

3.2.3.2 Intracrystalline plasticity

Pole figure plots show that omphacite developed a CPO with (010) poles perpendicular to the foliation while poles to (001) form a dispersed girdle within the foliation (Fig. 13). Again, the CPO seems to be dominated by the axis orientation of small grains since larger clasts show rather random orientated strong single point maxima (Fig. 13 centre). Again, misorientation axis plots show a point maximum parallel to [001] for smaller misorientations. Additionally, a slight increase in misorientation axis around (010) can be observed (Fig. 14). Pole figure plots of garnet show random point maxima (Fig. 15). The distribution of rotation axis is random and no maxima can be recognized (Fig. 16). Omphacite shows strain localisation in the form of both brittle and plastic deformation (Fig. 20A). Low angle grain boundaries occur more often than in the 25% garnet sample, both around cracks and in a distance to cracks. Planar features are also commonly found. Grains showing little to no misorientation are mostly smaller. The average misorientation of omphacite in the overview map (Fig. 20A) is 1.61. Garnet also shows a localisation of strain (Fig. 20B). It presents both, more brittle and plastic deformation than the 25% garnet sample. Larger grains seem to be less affected by both. Low angle grain boundaries occur mostly around cracks, though misorientations frequently occur independent of cracks as well.

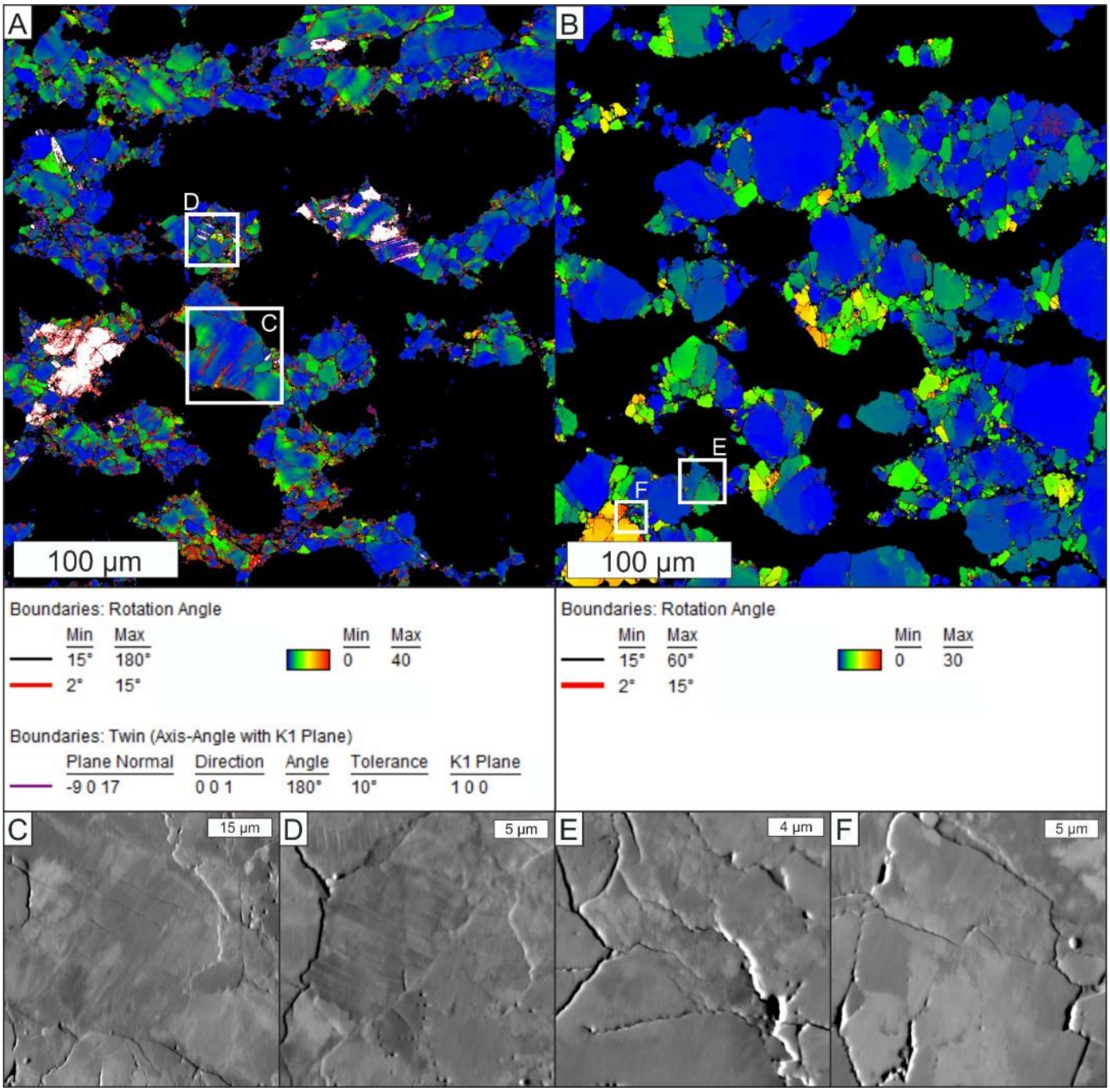

Figure 20. Misorientation deviation angle map of the deformed eclogite containing a 50% volume fraction of garnet. Low-angle (<15°) grain boundaries are in red, grain boundaries (>15°) in black and twins in omphacite are in purple. Inserted rectangles mark the locality of orientation contrast images C to F. A) Omphacite shows a smaller grain size at phase boundaries and when squeezed between garnet. Higher misorientation deviation angles and low-angle grain boundaries are also more common around grain boundaries. Larger omphacite clasts show linear features subparallel to the misorientation pattern. B) Smaller garnet grains tend to show higher misorientation angles. C) Linear feature in omphacite crosscut by cracks. D) Omphacite twins and low-angle grain boundaries. E), F) Irregular orientation contrast in garnet.

Where garnet is more deformed, the surrounding omphacite also shows higher degree in misorientation deviation angles, low-angle grain boundaries and sometimes recrystallisation. The average misorientation angle in the overview map (Fig. 20B) is 0.60.

3.2.3.3 Trace analysis of planar features

In this sample omphacite again exhibits planar features along (100) planes that show a misorientation change of 180° perpendicular to them (Fig. 20). Theses planar occur less often than in the 25%-garnet sample. Planar features showing sudden smaller changes in misorientation perpendicular to them also are found along (100) and (110) planes (Fig. 18). They again appear in form of straight lines or more irregular lamellae and misorientation profiles running parallel to them show a gradual change in misorientation. Additionally, there are some planar features which do not seem to match any of the previously mentioned planes. Some grains have planar features with two different orientations.

3.2.4 75% Garnet Sample

3.2.4.1 Microstructure

Deformed omphacite-garnet aggregates containing 75% volume fraction of garnet can be similar to the starting material characterized by interconnected framework of garnet surrounding omphacite clusters (Fig. 21A). Overall, the sample is highly fractured. In areas of the thin section where more omphacite is present garnet still tends to form layers. The largest intact garnet grains have diameters of up to 100 µm, have rounded grain boundaries and are circular to slightly elongated. Due to garnet being mostly fractured most grains are smaller and more angular. The average diameter is 3.10 µm. The average aspect ratio is 0.54. In the BSE images (Fig. 12E, F) garnet again shows chemical zoning with iron depleted, magnesium enriched rims. Fracturing of garnet occurs the most in this sample and in all directions. Straight, vertical fractures in garnet are rare. In omphacite enriched areas, larger omphacite grains of up 100 µm can be present, though they are rare. In smaller spaces between garnet layers omphacite is mostly fine grained with diameters of less than a micrometre.

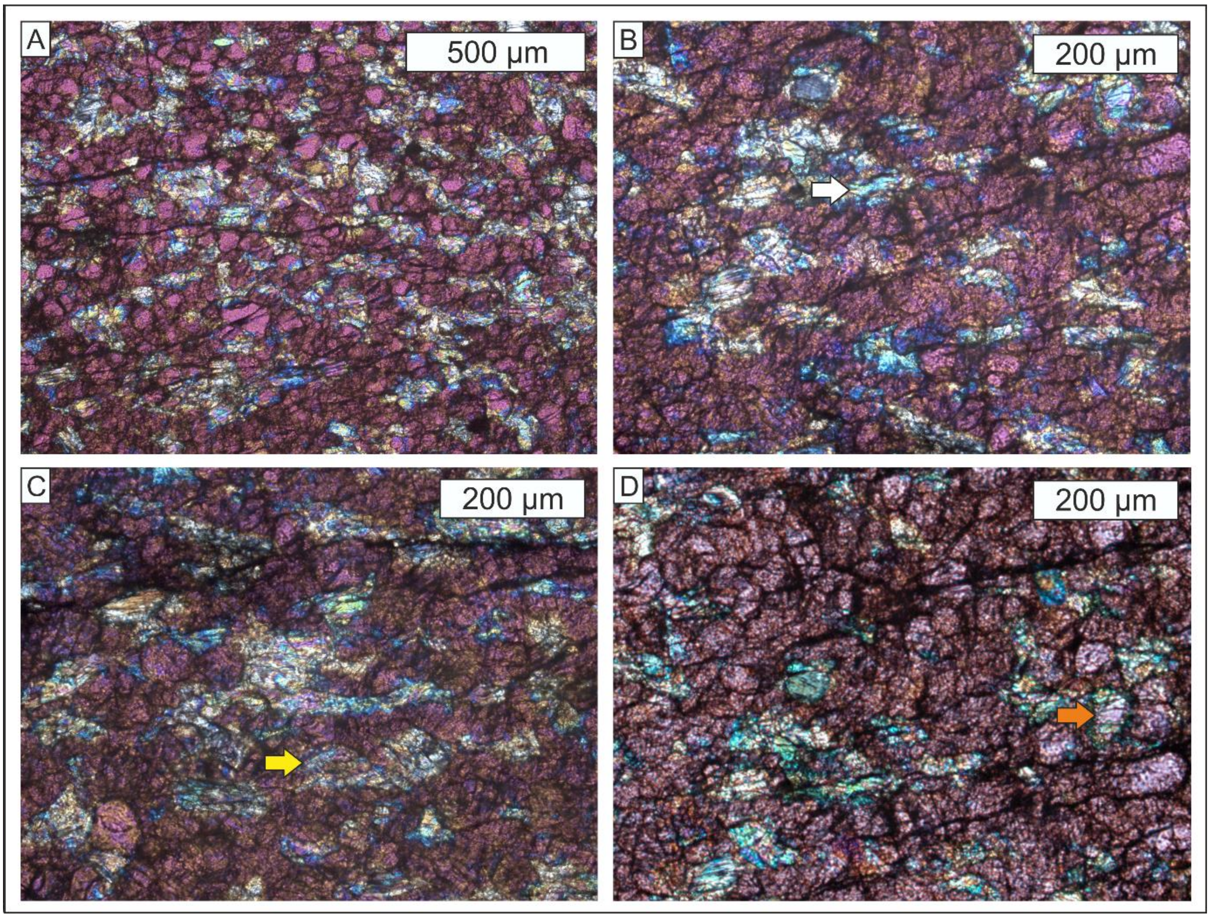

Figure 21. Optical microscope images of deformed eclogite containing a 75% volume fraction of garnet. Crossed polarizers and lambda plate inserted. A) The fabric is defined by garnet forming both larger clusters and layers. B) Where squeezed between garnet, omphacite is often either elongated (white arrow) or very fine grained. C) Some Omphacite grains show twinning. D) Garnet breaks completely randomly. Omphacite sometimes shows multiple parallel horizontal fractures (orange arrow).

Horizontally elongated omphacite grains can still be found though their orientation and shape seem to depend mostly on the surrounding garnet. The average diameter of omphacite in the overview EBSD (Fig. 22) map is 3.39 µm and the average aspect ratio is 0.49. Larger grains sometimes show twinning, most omphacite grains show undulatory extinction. The intracrystalline distortion is confirmed by an orientation contrast visible in BSE images. This sample shows the highest fracture density in omphacite. Larger accumulations of omphacite of around 100 µm in diameter may show horizontal fractures with somewhat regular spacing between them, with the horizontal fractures not quite reaching the surrounding garnet (Fig. 21D). Nevertheless, fracturing occurs overall random with no preferred orientation.

3.2.4.2 Intracrystalline plasticity

Pole figure plots of omphacite again show a CPO with (010) poles perpendicular to the foliation, which is mostly noticeable in grains with diameters less than 10 µm. Omphacite grains smaller than 10 µm also show a maximum of (001) poles, while larger grains show random point maxima (Fig. 13). Again, misorientation axis plots reveal a maximum parallel to [001] for smaller misorientations (Fig. 14). Pole figure plots of garnet show randomly distributed point maxima (Fig. 15). Axis plots reveal no point maxima (Fig 16). Omphacite again shows strain localisation in the form of both brittle and crystal plastic deformation, with brittle deformation being more common (Fig. 22A). Low angle grain boundaries occur mostly along cracks. Planar features are still common. Where omphacite forms thin layers within the garnet framework, the density of cracks and low angle grain boundaries tends to be noticeably higher. The average misorientation of omphacite in the EBSD map (Fig. 20A) is 1.98. Garnet also shows both brittle and plastic deformation (Fig. 20B). Again, the brittle deformation is most noticeable in this sample. Larger grains of 50 µm and more seem to be less effected by both. Low angle grains boundaries occur along cracks. Lower misorientations occur also independently of cracks, though the majority are tied to fracturing. The average misorientation of garnet in the overview map is 0.89 (Fig. 20B).

3.2.4.3 Trace Analysis of planar features

In the 75% garnet sample planar features occurring along (100) and (110) planes are again common. Misorientation profiles parallel to them reveal a gradual in- and decrease in misorientation, while misorientation profiles perpendicular to them show sudden changes in misorientation (Fig. 18). Some of the features tracing (100) planes show a 180° change in misorientation perpendicular to them. These are again less common than in the 25%- and 50%-garnet sample. Planar features matching well with (010) or (001) planes were not found and some match none of the mentioned planes.

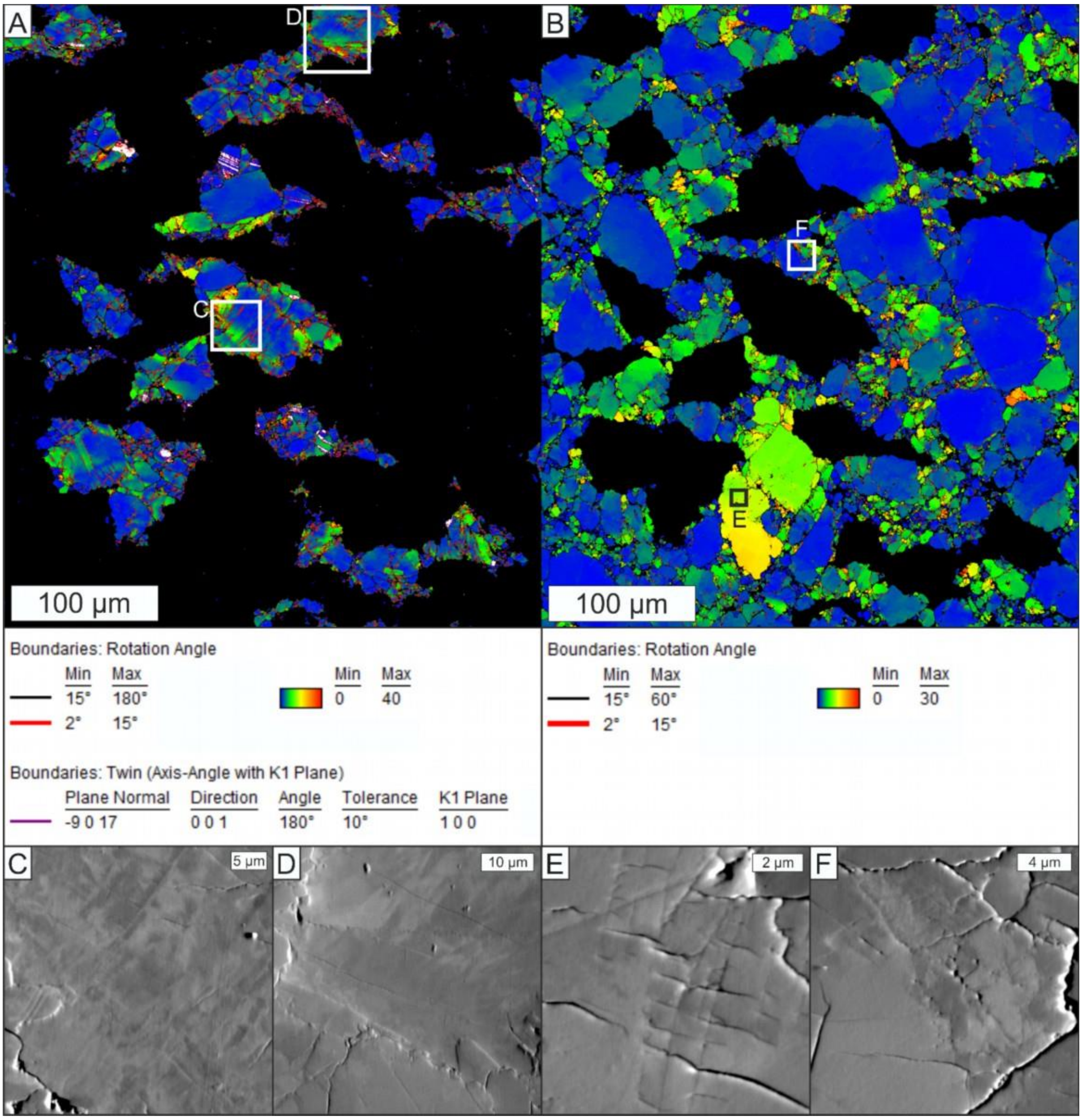

Figure 22. Misorientation deviation angle map of the deformed eclogite containing a 75% volume fraction of garnet. Low-angle (<15°) grain boundaries are in red, grain boundaries (>15°) in black and twins in omphacite are in purple. Inserted rectangles mark the locality of orientation contrast images C to F. A) Omphacite shows a smaller grain size at phase boundaries and when squeezed between garnet Also, the crystal distortion tends to be higher at phase boundaries indicated by higher misorientation deviation angle and increased low-angle grain boundaries. Larger omphacite clasts show linear features subparallel to the misorientation pattern. B) Larger garnet clasts show a low misorientation deviation angle while smaller grains tend to be higher strained. C) Irregular orientation contrast in omphacite with two sets of linear features. D) Irregular orientation contrast pattern in omphacite crosscut by cracks. E) En-echelon micro-cracks in garnet. F) Irregular orientation contrast in garnet crosscut by micro-cracks (white arrow).

3.3 Summary

With increasing garnet content, we can see a change from a slight foliation made up of horizontal to sub-horizontal garnet layers at a 25% volume fraction of garnet to a more defined foliation consisting of interconnected, horizontal garnet and omphacite layers at a 50% volume fraction of garnet to a loadbearing garnet framework at 75% garnet content. Similar microstructures can be found in all samples, though their abundance varies depending on phase abundance. With increasing garnet content fractures increase in both omphacite and garnet. Especially in garnet a transition from predominantly vertical fractures to fracturing occurring in all directions can be seen. Undulatory extinction of omphacite is common in all samples, while planar features with a 180° change in misorientation in omphacite appear less often with increasing garnet content. The omphacite CPO changes as well and is actually most prominent in the sample containing a 50% volume. In Omphacite higher misorientation deviation angles and low angle grain boundaries occur mostly close to phase boundaries and around cracks. Especially between the 25% garnet and 50% sample an increase in low angle grain boundaries can be seen. Lower grainsizes of omphacite are also often found close to phase boundaries. Larger omphacite clasts often show planar features with increased misorientation, which often trace the 100 and 110 planes. In garnet higher misorientation occur mostly in smaller grains. For both phases the average grainsize decreases with increasing garnet content, while the average misorientation increases.

4. Discussion

4.1 Deformation mechanisms

4.1.1 Garnet

In all eclogite samples garnet predominantly deforms by brittle deformation. Fracturing of garnet can be observed throughout all samples, however, the number of fractures increases with increasing garnet content in eclogite. The most noticeable change in brittle deformation of garnet is between the 25%-garnet sample and the 50%-garnet sample. In the sample containing a 25% volume fraction garnet breaks mainly parallel to the main compressive stress. With increasing garnet content, fractures become not just more frequent but also more random in orientation. This could be due to a concentration of stress in garnet aggregates, causing local perturbations in the overall stress field and garnet to break more randomly (Yamato et al., 2019). Another possible reason could be a rotation of garnet during the deformation experiments, changing its orientation in respect to the stress field.

Aside of fracturing, garnet crystals show indication of minor crystal plastic deformation. Misorientations in garnet are mostly found around cracks, similarly to garnet in naturally deformed eclogite where dislocations are also found around cracks and dislocation nucleation is assisted by the stress concentration at the crack tips (Voegelé et al., 1998a; Rogowitz et al., 2018). Higher misorientation deviation angles are mostly found in smaller grains, though with increasing garnet content larger grains show increasingly higher misorientation angles as well. This increase of misorientation could be due to an increase of crystal plastic deformation of garnet. Another reason could be that misorientations are mostly associated with fractures, and the number of fractures also increases with increasing garnet content.

4.1.2 Omphacite

Microstructures observed in all samples like undulatory extinction, and planar features, that are likely slip lines, as well as a CPO indicate, that the main crystal plastic deformation mechanism is likely dislocation creep. While these microstructures are found in similar amounts in all samples, the CPO is actually most noticeable in the 50%-garnet sample, suggesting that omphacite might have experienced more dislocation creep at 50% volume fraction of garnet. Still, the average misorientation is actually highest in the 75%-garnet sample, which might be because some misorientation is tied to fracturing (Boland and Tullis, 1986).

Another crystal plastic deformation mechanism observed in the deformed omphacite is likely mechanical twinning, as planar features parallel to (100) with a 180° change in misorientation were found in all samples. A clear dependence on garnet content can be observed as twins decrease with increasing garnet content. As the volume fraction of garnet increases, the number of twins decreases, especially between the 25%- and 50%- garnet fraction sample.

Low angle grain boundaries are also found in all samples and increase in between the 25%-garnet and 50%-garnet sample. They are also commonly found close to phase boundaries, as are grains of smaller sizes and increased misorientation, indicating a localization of strain at phase boundaries. This could be, because the strong competence contrast between garnet and omphacite creates a heterogeneity, where strain can localize (Holyoke and Tullis, 2006; Czaplińska et al., 2015).

Overall, the deformational behaviour of omphacite changes from predominantly crystal plastic to more brittle dominated with increasing garnet. Unlike in garnet, the orientation of fractures is random in all samples.

4.1.2.1 Omphacite texture development

Omphacite in all deformed eclogite samples exhibit a texture resembling a S-Type CPO. It is most noticeable in the 50% garnet sample. A CPO can be formed by dislocation creep but has also been shown to form by diffusion and dissolution-reprecipitation creep (Mauler et al., 2001; Stünitz et al., 2020). Microstructures in omphacite like undulatory extinction and slip lines, which will be discussed in more detail below, indicate that the CPO here is likely caused by dislocation creep.

Omphacite in all samples exhibits multiple planar features. Some of them can be identified as deformation twins, as they exhibit the typical 180° change in orientation and are parallel to (100) planes (Moghadam et al., 2010). These noticeably decrease with increasing garnet content. Deformation twins are also a common feature in naturally and experimentally deformed omphacite and have been observed to form at a wide range of temperature and strain rate conditions (van Roermund and Boland, 1981; Müller and Franz, 2008). In the 25%-garnet sample omphacite twin density appears higher when compared to the 50%- and 75%-garnet sample. Twins can be found throughout all grain sizes, however they affect mostly smaller grains in samples with a garnet content of 50% and above. A continuous change in misorientation can be observed parallel to some twins, indicating that deformation creep could have occurred along the twin planes.

The other planar features do not show a 180° change in orientation perpendicular to them, but only one of a few degrees. Most follow (010) and (110) planes. Some trace (100) and (001) planes as well. Similar features parallel to (010) and (110) have also been found in omphacite in naturally deformed eclogite (Müller and Compagnoni, 2009). Faults parallel to (010) have been identified as chain multiplicity faults, which were formed by stress-induced dissociation of [011] dislocations (Müller et al., 2004). The planar features observed here are usually accompanied by a continuous misorientation gradient, suggesting that they are slip lines. The (110) planes are also cleavage planes in omphacite, so slip might have occurred along cleavage planes. A few grains show slip lines paralleling two different directions and crosscutting each other, indicating multiple slip systems to be active. The observation of multiple slip systems is in accordance with transmission-electron microscopy studies on omphacite which have identified (100) [001], {110} [001], {110} ½, and {-110} ½ to be active (Godard and van Roermund, 1995). It has been proposed that a combination of those slip systems, rather than slip on one slip system, is resulting in the often-observed S-Type CPO in omphacite (Godard and van Roermund, 1995). The identified slip systems also match well with the here observed slip lines.

4.1.3 Eclogite

Only few deformation experiments have been conducted on eclogite regarding the influence of the volume fraction of its two main phases (e.g., Zhang and Green, 2007) even though deformation experiments on other two-phase aggregates have previously demonstrated that phase distribution can affect a rocks rheology and deformational behaviour (e.g., Jordan, 1987; Tullis et al., 1991; Ji et al., 2001). This is also the case for eclogite as demonstrated by my study. As the volume fraction of garnet increases, the deformational behaviour of eclogite changes from predominantly crystal plastic deformation of omphacite through mostly dislocation creep and twinning and almost rigid behaviour of garnet to brittle deformation of both, garnet and omphacite. This could indicate that stress mostly concentrates in omphacite in the 25%-garnet sample and partitions more and more into garnet as garnet content increases. This would be in line with Handys (1994) theory that stress concentrates in the interconnected weak phase in IWLs, which are here represented by the 25% garnet sample. In a LBFs, which match the fabric of the 75%-garnet sample, stress concentrates in the LBF and strain rates are nearly uniform. Another factor influencing deformational behaviour besides phase distribution, seem to be phase contacts. The strong competence contrast between garnet and omphacite seems to lead to a heterogeneity, and subsequently a localization of strain in omphacite. As a result, an increase in misorientation as well as low angle grain boundaries can be found in omphacite at phase boundaries.

4.2 Eclogite rheology

It has previously been proposed that the strength of two-phase increases with an increasing volume fraction of the stronger phase (Tullis et al., 1991). This has been further confirmed with multiple deformation experiments, for example on calcite-quartz aggregates (Rybacki et al., 2003) and anorthite-diopside rocks (Dimanov and Dresen, 2005), as well as eclogite (Zhang and Green, 2007), where the strength of eclogite increased with increasing garnet content. This is also in line with the results of the deformation experiments presented here. The mechanical data shows an increase in strength with increasing garnet content. Additionally, peak differential stress is reached at a higher strain with increasing garnet content. Especially between the sample containing a 25% volume fraction of garnet and the sample containing a 50% volume of garnet a significant increase in strength can be observed. A similar increase would be expected between the 50%- and 75%-garnet sample, however the initial increase is lower than in the other samples and the final strength is not much higher than that of the 50%-garnet sample, so the strength of the 75%-garnet sample might not be representative of all eclogite containing a 75% volume fraction of garnet.

After maximum differential stress is reached, the mechanical data of all samples indicates mechanical weakening, which is likely due to embrittlement (Labuz et al., 2018). This suggests that the main weakening mechanism at the given deformational conditions is brittle failure. It should be noted, that the differential stress drop the mechanical data shows for the 50%-garnet sample is a lot more significant than the other samples. This could be due to a shear fracture which formed on the bottom half of the sample during the experiment. As microscopy images and EBSD data were acquired in areas not affected by the shear fracture, the data can still be considered representative up to peak compressive strength of the sample.

5. Conclusion

In this study synthetic eclogites containing a 25%, 50% and 75% volume fraction of garnet have been deformed with a Griggs-type deformation apparatus. Microstructural analysis was conducted though optical and scanning electron microscopy, including backscattered electron imaging, forward scattered electron imaging and electron backscattered diffraction mapping to determine the deformational behaviour of eclogite and its dependence on the volume fractions of its main phases, garnet and omphacite. The main conclusions are:

- The strength of eclogite increases with increasing garnet content.
- The deformational behaviour changes from predominantly crystal plastic deformation of mostly omphacite to increasingly more brittle deformation of both phases with increasing garnet content.
- Garnet shows signs of both crystal plastic and brittle deformation. Brittle deformation of garnet increases significantly with increasing garnet content.
- The predominant plastic deformation mechanism of omphacite is dislocation creep on multiple slip systems.
- Strain localizes at phase boundaries.

References

Angiboust, S., Agard, P., Raimbourg, H., Yamato, P., & Huet, B. (2011). Subduction interface processes recorded by eclogite-facies shear zones (Monviso, W. Alps). Lithos, 127(1-2), 222–238.

Angiboust, S., Agard, P., Yamato, P. & Raimbourg, H. (2012). Eclogite breccias in a subducted ophiolite: A record of intermediate-depth earthquakes?. Geology. 40. 707-710. 10.1130/G32925.1.

Austrheim, H. (1987). Eclogitization of lower crustal granulites by fluid migration through shear zones. Earth and Planetary Science Letters, 81(2-3), 221–232.

Austrheim, H., Erambert, M., & Engvik, A.K. (1997). Processing of crust in the root of the Caledonian continental collision zone: the role of eclogitization. Tectonophysics, 273(1- 2), 129–153.

Austrheim, H., Corfu, F., Bryhni, I., & Andersen, T.B. (2003). The Proterozoic Hustad igneous complex: A low strain enclave with a key to the history of the Western Gneiss Region of Norway. Precambrian Research, 120(1-2), 149–175.

Austrheim, H. (2013). Fluid and deformation induced metamorphic processes around Moho beneath continent collision zones: Examples from the exposed root zone of the Caledonian mountain belt, W-Norway. Tectonophysics, 609(0040), 620–635.

Bestmann, M., Habler, G., Heidelbach, F. & Thöni, M., (2008). Dynamic recrystallization of garnet and related diffusion processes. Journal of Structural Geology, 30, 777–790.

Buatier, M., van Roermund, H.M.L., Drury, M.R. & Lardeaux, J.M. (1991). Deformation and recrystallization mechanisms in naturally deformed omphacites from the Sesia-Lanzo zone; geophysical consequences. Tectonophysics, 195(1), 11-27.

Bucher, K. (2005). METAMORPHIC ROCKS | Facies and Zones, Editor(s): Richard C. Selley, L. Robin M. Cocks, Ian R. Plimer, Encyclopedia of Geology, Elsevier, 402-409.

Boland, J.N. & Tullis, T.E. (1986). Deformation Behavior of Wet and Dry Clinopyroxenite in the Brittle to Ductile Transition Region. In Mineral and Rock Deformation (eds B. Hobbs and H. Heard), 36, 35–49.

Bystricky, M. & Mackwell, S. (2001). Creep of dry clinopyroxene aggregates. Journal of Geophysical Research, 106, 13443– 13454.

Cao, Y., Du, J., Park, M., Jung, S., Park, Y., Kim, D., et al. (2020). Metastability and nondislocation-based deformation mechanisms of the Flem eclogite in the Western Gneiss Region, Norway. Journal of Geophysical Research: Solid Earth, 125, e2020JB019375.

Czaplińska, D., Piazolo, S. & Zibra, I. (2015). The influence of phase and grain size distribution on the dynamics of strain localization in polymineralic rocks. Journal of Structural Geology, 72, 15-32.

Dimanov, A., & Dresen, G. (2005). Rheology of synthetic anorthite-diopside aggregates: Implications for ductile shear zones, Journal of Geophysical Research, 110, B07203, doi:10.1029/2004JB003431.

Druiventak, A., Trepmann, C., Renner, J. & Hanke, K. (2011). Low-temperature plasticity of olivine during high stress deformation of peridotite at lithospheric conditions — An experimental study. Earth and Planetary Science Letters - Earth Planet. Sci. Lett. 311, 199–211.

Engvik, A.K., Andersen, T.B., & Wachmann, M. (2007). Inhomogeneous deformation in deeply buried continental crust, an example from the eclogite-facies province of the Western Gneiss Region, Norway. Norsk Geologisk Tidsskrift, 87(4), 373–389.

Godard, G. & van Roermund, H.L.M. (1995). Deformation-induced clinopyroxene fabrics from eclogites. Journal of Structural Geology, 17, 1425-1443.

Green, D.H. & Ringwood, A.E. (1967). An experimental investigation of the gabbro to eclogite transformation and its petrological applications. Geochimica et Cosmochimica Acta, 31(5), 767-833.

Griggs, D. (1967). Hydrolytic weakening of quartz and other silicates. Geophysical Journal of the Royal Astronomical Society, 14(1-4), 19–31.

Handy, M.R. (1994). Flow laws for rocks containing two non-linear viscous phases: A phenomenological approach, Journal of Structural Geology, 16, 287–301.

Haüy, R. J., 1822. Traité de Minéralogie (Second edition), revue, corrigée, considérablement augmentée par l'auteur. Bachelier et Huzard, Paris.

Helmstaedt, H., Anderson, D. L. & Gavasci, A. T. (1972). Petrofabric studies of eclogite, spinel websterite, and spinel-lherzolite xenoliths from kimberlite-breccia pipes in southeastern Utah and northeastern Arizona. Journal of Geophysical Research, 77, 4350–4365.

Holyoke, C.W. III & Tullis, J. (2006). Mechanisms of weak phase interconnection and the effects of phase strength contrast on fabric development. Journal of Structural Geology, 621-640.

Ji, S., Wang, Z. & Wirth, R. (2001). Bulk flow strength of forsterite–enstatite composites as a function of forsterite content, Tectonophysics, 341, 69–93.

Jolivet, L., Raimbourg, H., Labrousse, L., Avigad, D., Leroy, Y., Austrheim, H., & Andersen, T.B. (2005). Softening trigerred by eclogitization, the first step toward exhumation during continental subduction. Earth and Planetary Science Letters, 237(3-4), 532–547.

Jordan, P.G. (1987). The deformational behaviour of bimineralic limestone-halite aggregates. Tectonophysics, 135, 185–197.

Karato, S., Wang, Z., Liu, B., & Fujino, K. (1995). Plastic deformation of garnet: systematics and implications for the rheology of the mantle transition zone. Earth and Planetary Science Letters, 130, 13–30.

Keppler, R., Stipp, M., Behrmann, J.H., Ullemeyer, K. & Heidelbach, F. (2016). Deformation inside a paleosubduction channel—insights from microstructures and crystallographic preferred orientations of eclogites and metasediments from the Tauern Window, Austria. Journal of Structural Geology, 82, 60-79.

Keppler, R. (2018). Crystallographic preferred orientations in eclogites – A review. Journal of Structural Geology, 115, 284-296.

Kurz, W. (2005). Constriction during exhumation: evidence from eclogite microstructures. Geology, 33 (1), 37-40.

Labuz, J.F., Zeng, F., Makhnenko, R. & Li, Y. (2018). Brittle failure of rock: A review and general linear criterion, Journal of Structural Geology, 112, 7-28.

Le Goff, E. & Ballèvre, M. (1990). Geothermobarometry in albite-garnet orthogneisses: A case study from the Gran Paradiso nappe (Western Alps). Lithos, 25(4), 261-280.

Mauler, A., Godard, G. & Kunze, K. (2001). Crystallographic fabrics of omphacite, rutile and quartz in Vendée eclogite (Armorican Massif, France): Consequences for deformation mechanisms and regimes. Tectonophysics, 342, 81–112.

Miller, C., Konzett, J., Tiepolo, M., Armstrong, R.A., & Thöni, M. (2007). Jadeite-gneiss from the Eclogite Zone, Tauern Window, Eastern Alps, Austria: Metamorphic, geochemical and zircon record of a sedimentary protolith. Lithos, 93(1-2), 68–88.

Moghadam, R. H., Trepmann, C.A., Stöckhert, B., & Renner, J. (2010). Rheology of synthetic omphacite aggregates at high pressure and high temperature. Journal of Petrology, 51(4), 921–945.

Müller, W.F., Brenker, F.E., Barnert, E.B., Franz, G. (2004). Chain multiplicity faults in deformed omphacite from eclogite. European Journal of Mineralogy 16, 37–48.

Müller, W.F. & Franz, G. (2008). TEM-microstructures in omphacite and other minerals from eclogite near to thrust zone; the Eclogite Zone–Venediger nappe area, Tauern Window, Austria. Neues Jahrbuch für Mineralogie Abhandlungen, 184, 285–298.

Müller, W. & Compagnoni, R. (2009). Eclogite from the ultrahigh-pressure metamorphic unit at Lago di Cignana, Western Alps: A process-oriented transmission electron microscope study. Lithos, 109. 323-332.

Philippot, P. & van Roermund, H.L. (1992). Deformation processes in eclogitic rocks: evidence for the rheological delamination of the oceanic crust in deeper levels of subduction zones. Journal of Structural Geology, 14(8-9), 1059–1077.

Prior, D.J., Wheeler, J., Brenker, F.E., Harte, B. & Matthews, M. (2000). Crystal plasticity of natural garnet: new microstructural evidence. Geology, 28, 1003–1006.

Ringwood, A.E. & Green, D.H., (1966). An experimental investigation of the gabbro-eclogite transformation and some geophysical implications. Tectonophysics, 3, 383–427.

Ringwood, A.E. (1991). Phase transformations and their bearing on the constitution and dynamics of the mantle. Geochimica et Cosmochimica Acta, 55, 2083-2110.

van Roermund, H.L.M. & Boland, J.N. (1981). The dislocation substructures of natural deformed Omphacite. Tectonophysics, 78, 403-418.

Rogowitz, A., Dubosq, R. & Zaefferer, S. (2018). Direct observation of dislocation nucleation in pyrite using combined electron channelling contrast imaging and electron backscatter diffraction. Terra Nova, 30(6), 423-430.

Rogowitz, A. & Huet, B. (2021). Evolution of fluid pathways during eclogitization and their impact on formation and deformation of eclogite: A microstructural and petrological investigation at the type locality (Koralpe, Eastern Alps, Austria). Tectonophysics, 819, 229079.

Rybacki, E., Paterson, M., Wirth, R. & Dresen, G. (2003). Rheology of calcite-quartz aggregates deformed to large strain in torsion. Journal of Geophysical Research ,108, 2089.

Rybacki, E., Renner, J., Konrad, K. et al. (1998). A Servohydraulically-controlled Deformation Apparatus for Rock Deformation under Conditions of Ultra-high Pressure Metamorphism. Pure appl. geophys. 152, 579–606.

Smit, M. A., Scherer, E. E., John, T., & Janssen, A. (2011). Creep of garnet in eclogite: Mechanisms and implications. Earth and Planetary Science Letters, 311(3-4), 411–419.

Stünitz, H., Neufeld, K., Heilbronner, R., Finstad, A., Konopasek, J. & Mackenzie, J. (2020). Transformation weakening: Diffusion creep in eclogites as a result of interaction of mineral reactions and deformation. Journal of Structural Geology, 139, 104129.

Tullis, T.E., Horowitz, F.G., and Tullis, J. (1991). Flow laws of polyphase aggregates from end-member flow laws, Journal of Geophysical Research, 96, 8081–8096.

Voegelé, V., Cordier, P., Sautter, V., Sharp, T. G., Lardeaux, J. M., & Marques, F. O. (1998a). Plastic deformation of silicate garnets. II. Deformation microstructures in natural samples. Physics of the Earth and Planetary Interiors, 108(4), 319–338.

Voegelé, V., Ando, J. I., Cordier, P., & Liebermann, R. C. (1998b). Plastic deformation of silicate garnets. I. High-pressure experiments. Physics of the Earth and Planetary Interiors, 108(4), 305–318.

Wang, Z. & Ji, S. (1999). Deformation of silicate garnets: Brittleductile transition and its geological implications. Canadian Mineralogist, 37, 525–541.

Xu, L., Mei, S., Dixon, N., Jin, Z., Suzuki, A.M., & Kohlstedt, D.L. (2013). Effect of water on rheological properties of garnet at high temperatures and pressures. Earth and Planetary Science Letters, 379, 158–165.

Yamato, P., Duretz, T., & Angiboust, S. (2019). Brittle/ductile deformation of eclogites: Insights from numerical models. Geochemistry, Geophysics, Geosystems, 20, 3116– 3133.

Zhang, J., Green, H.W., & Bozhilov, K.N. (2006). Rheology of omphacite at high temperature and pressure and significance of its lattice preferred orientations. Earth and Planetary Science Letters, 246(3-4), 432–443.

Zhang, J., & Green, H.W. (2007). Experimental investigation of eclogite rheology and its fabrics at high temperature and pressure. Journal of Metamorphic Geology, 25(2), 97– 115.

Appendix

I. Locations of the EBSD maps in the thin sections

Sample: D18 - 25% garnet

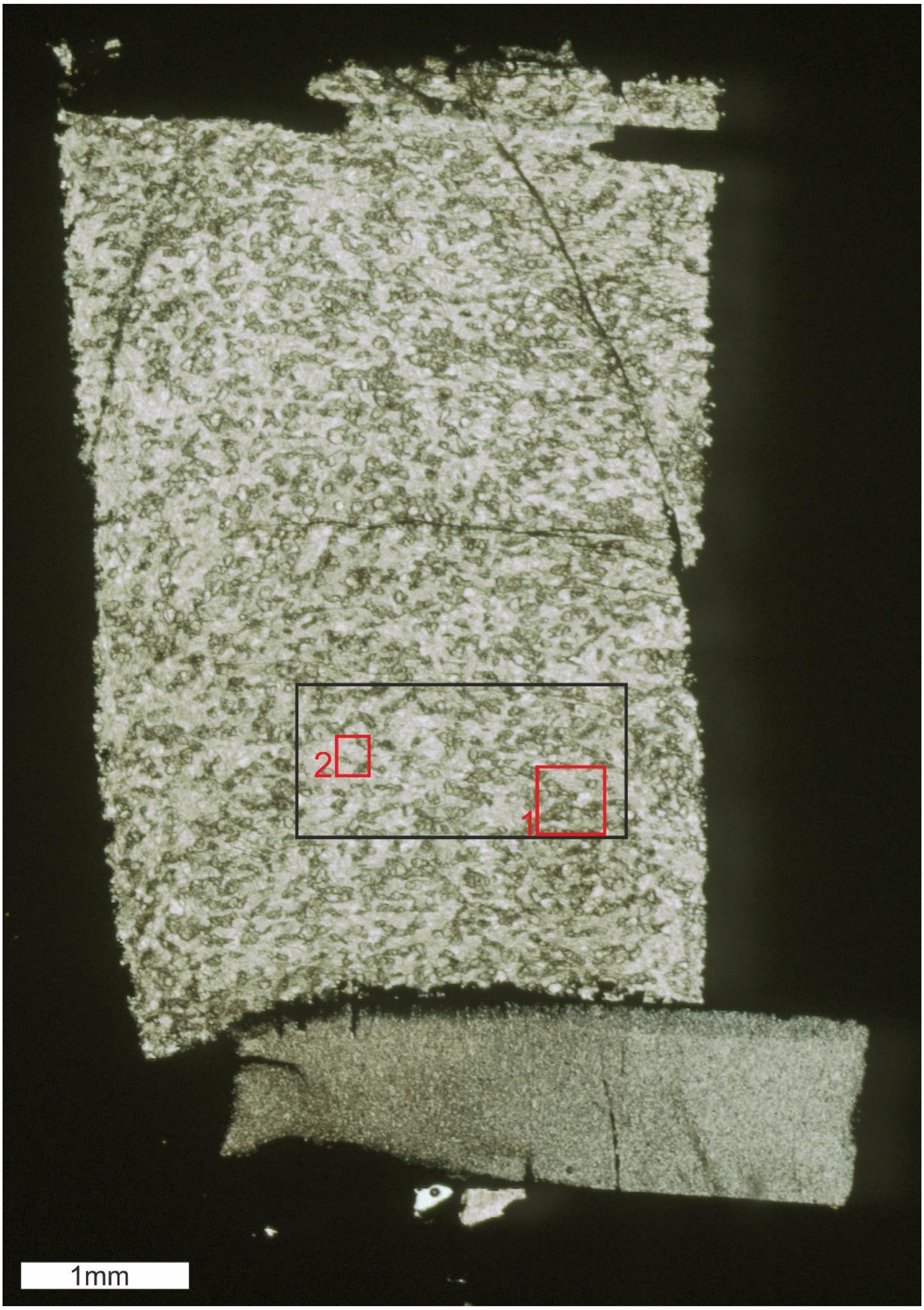

Scan of the 25%-garnet sample. The black square marks the location of the microscope images below. Red square 1 is the location of the overview map (Fig. 17), red square 2 is the location of the detail map (Fig. 18, top).

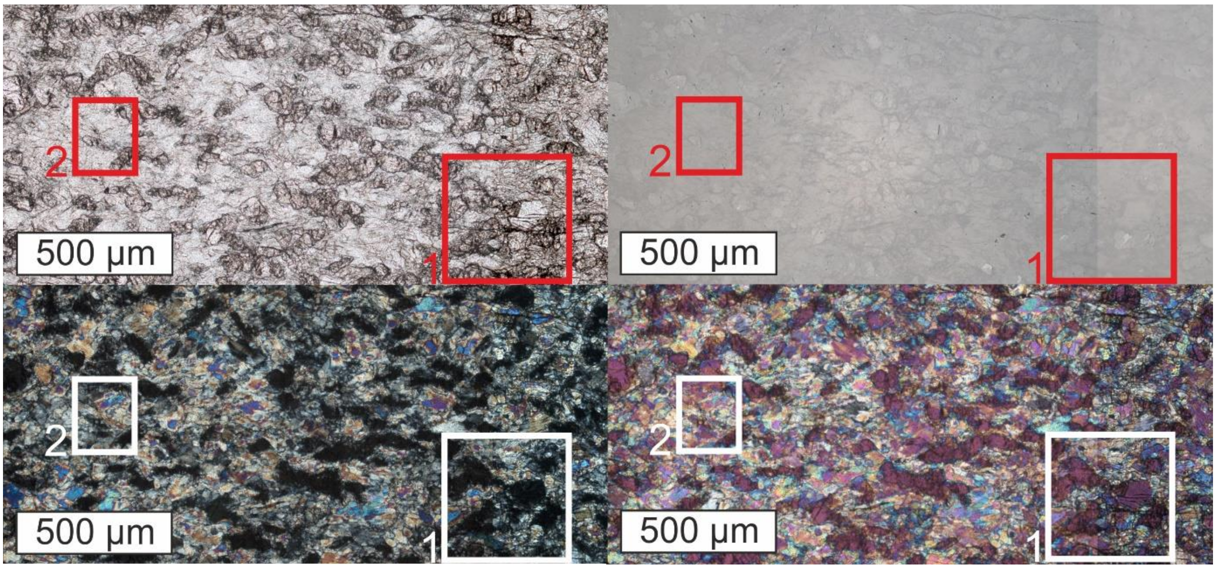

Images of the 25%-garnet sample taken with polarized light, reflected light, cross-polarized light and the lambda plate inserted. Square 1 marks the location of the overview map (Fig. 17), square 2 the location of the detail map (Fig. 18, top).

Sample: D19 – 50% garnet

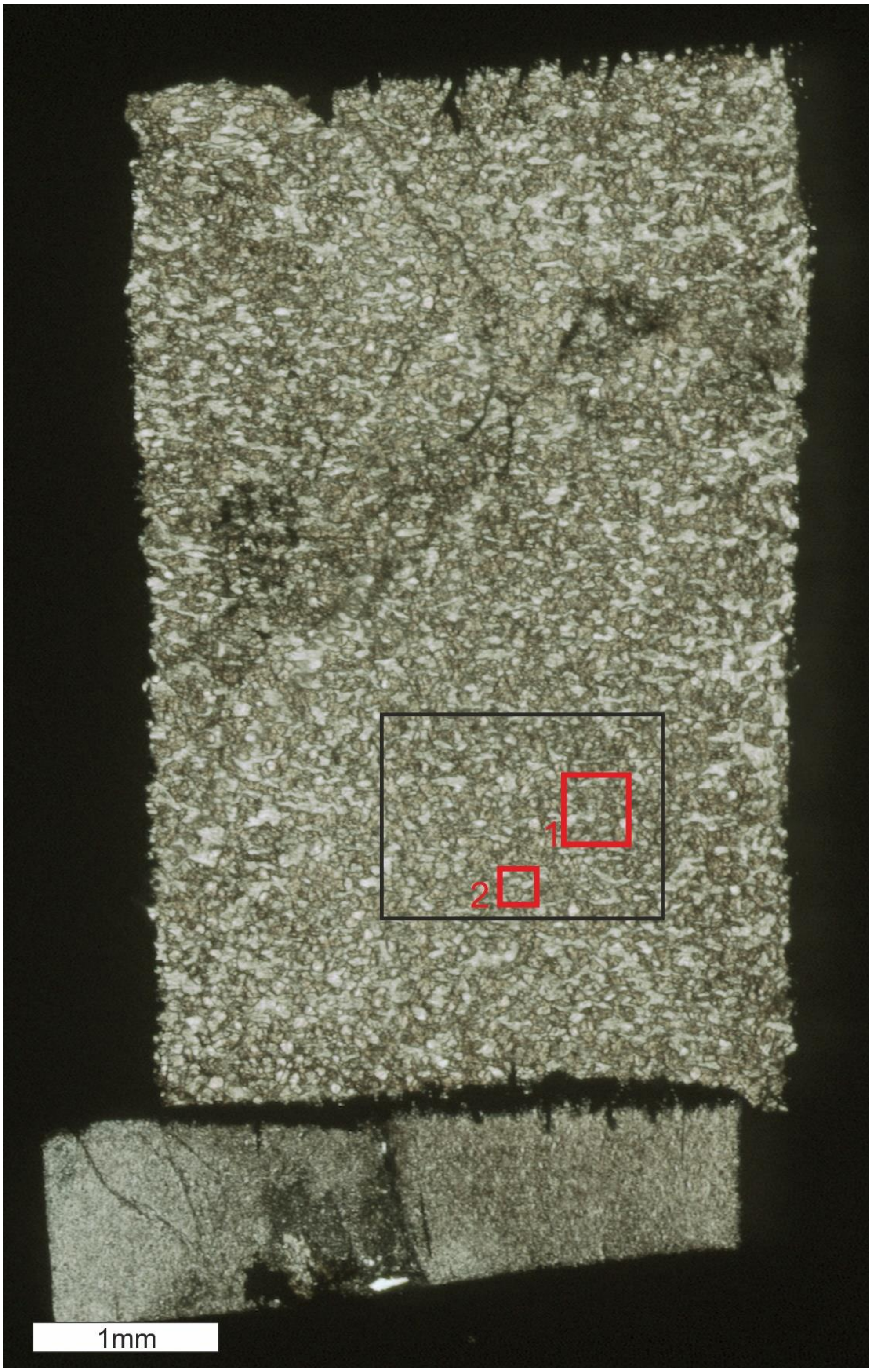

Scan of the 50%-garnet sample. The black square marks the location of the microscope images below. Red square 1 is the location of the overview map (Fig. 20), red square 2 is the location of the detail map (Fig. 18, middle).

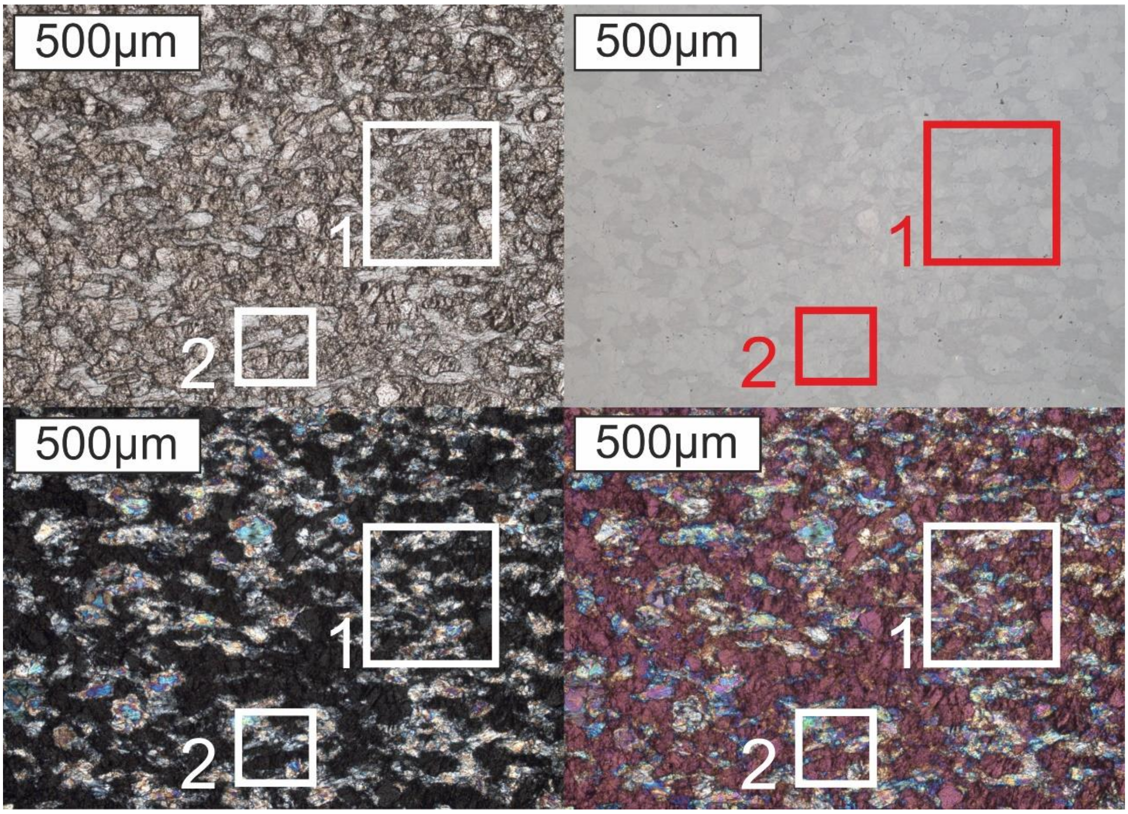

Images of the 50%-garnet sample taken with polarized light, reflected light, cross-polarized light and the lambda plate inserted. Square 1 marks the location of the overview map (Fig. 20), square 2 the location of the detail map (Fig. 18, middle).

Sample: D16 – 75% garnet

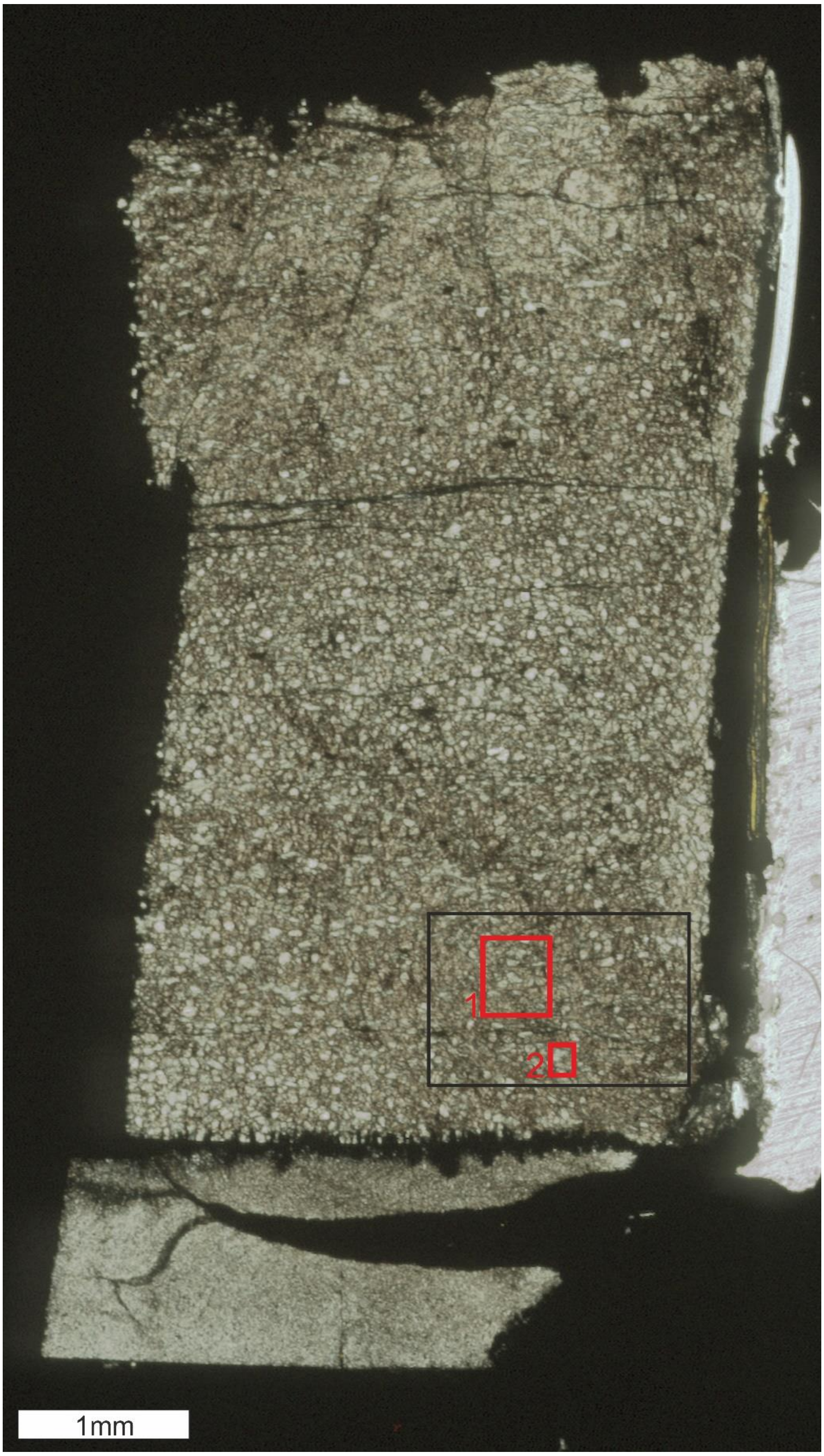

Scan of the 75%-garnet sample. The black square marks the location of the microscope images below. Red square 1 is the location of the overview map (Fig. 22), red square 2 is the location of the detail map (Fig. 18, bottom).

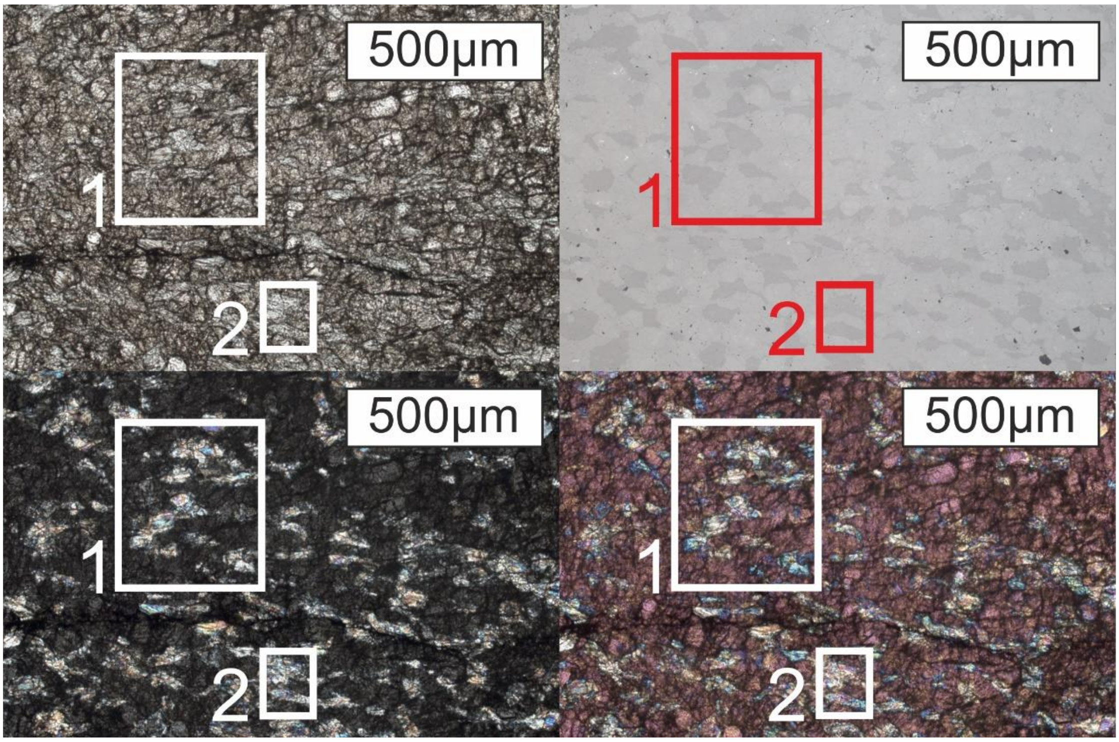

Images of the 75%-garnet sample taken with polarized light, reflected light, cross-polarized light and the lambda plate inserted. Square 1 marks the location of the overview map (Fig. 22), square 2 the location of the detail map (Fig. 18, bottom).

Sample: S28 – Top: 25% garnet, Bottom: 75% garnet

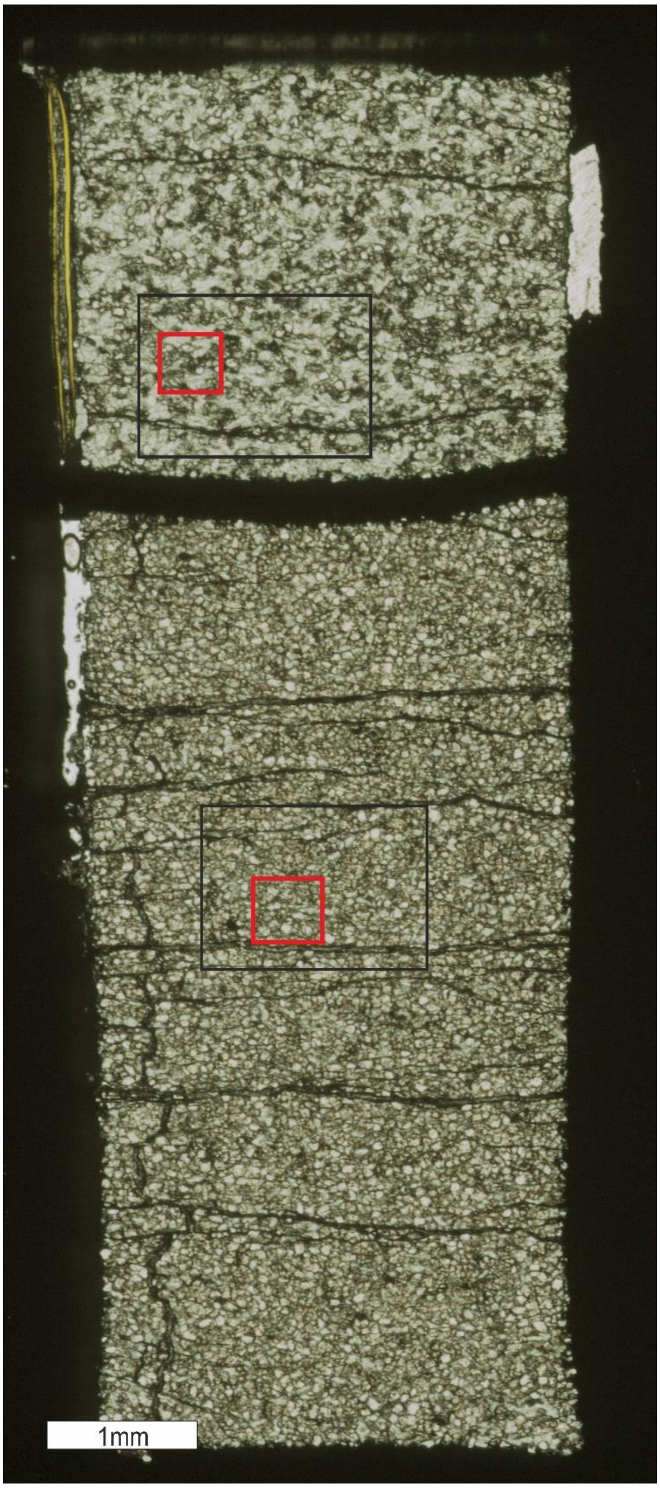

Scan of the starting material. The black square at the top marks the location of the microscope images of the starting material containing 25% garnet below. The red square at the top is the location of the EBSD map of the 25%-garnet starting material (Fig. 9A, B). The black square at the bottom marks the location of the microscope images of the starting material containing 75% garnet below. The red square at the bottom is the location of the overview map of the 75%-garnet starting material (Fig. 9C, D).

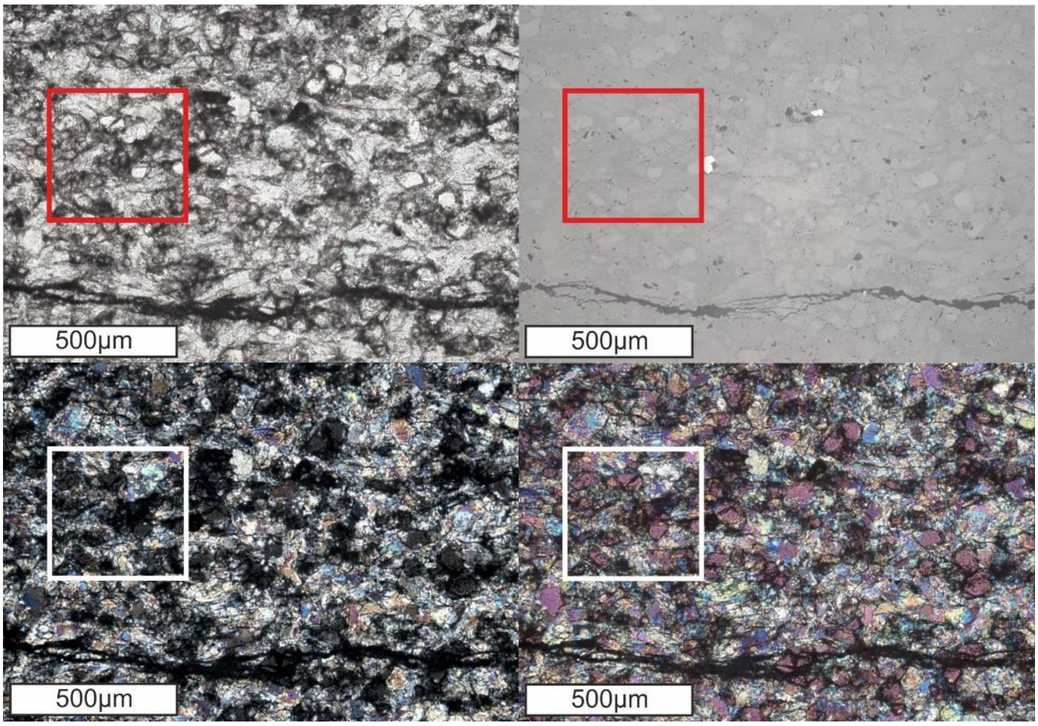

Images of the 25%-garnet starting material taken with polarized light, reflected light, cross-polarized light and the lambda plate inserted. The square marks the location of the overview map (Fig. 9A, B).

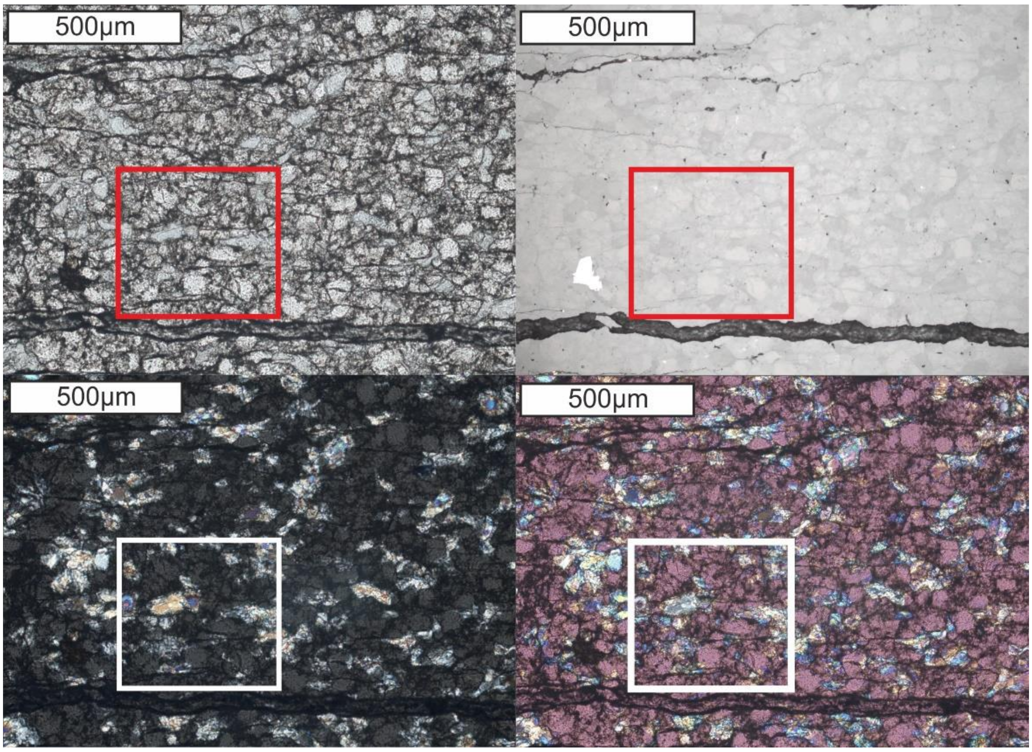

Images of the 75%-garnet starting material taken with polarized light, reflected light, cross-polarized light and the lambda plate inserted. The square marks the location of the overview map (Fig. 9C, D).